Unmanned Systems, Vol. 14, No. 2 (2026) 323–340

DOI: 10.1142/S2301385026500020

UNMANNED SYSTEMS
https://www.worldscientific.com/worldscinet/us

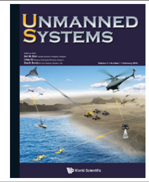

Self-Triggered Formation Control of an Asynchronous Multiple Underwater Unmanned Vehicle Under Communication Delay

Zheping Yan, Jinyu Yan*

College of Intelligent Systems
Science and Engineering,
Harbin Engineering University,
No. 145, Nantong Street, Harbin,
Heilongjiang 150001, China

To address the problem of multiple underwater unmanned vehicle (UUV) formation tracking under bounded communication delay, considering the existence of model parameter perturbations of UUVs as well as external ocean current disturbances, a distributed robust model predictive controller (DRMPC) with a dual closed-loop control structure and self-triggering mechanism is proposed. Among them, the outer-loop controller transforms the target trajectory into the target speed required by the inner-loop controller, and the inner-loop controller solves the effects of model parameter perturbations and bounded disturbances by RMPC and a finite-time extended state observer (FESO). To reduce the communication load of the system, a self-triggering mechanism is designed to determine the next triggering moment while solving the outer-loop optimization problem. The feasibility and stability of this controller are analyzed via mathematical induction and the ISpS Lyapunov theory. Finally, the effectiveness of this formation controller is validated through simulation experiments with multi-UUV.

Keywords: Underwater unmanned vehicle; formation trajectory tracking; asynchronous communication; self-triggering mechanism; distributed robust model predictive control.

1. Introduction

Since entering the 21st century, technological development has accelerated the consumption of energy, fossil energy sources are becoming increasingly depleted, and countries around the world are competing to begin to recognize and explore the ocean [1, 2]. However, complex marine environments, such as those characterized by communication difficulties, dimness, high pressure, and corrosiveness, hinder human exploration of the ocean, and UUV technology has become an important means for ocean exploration because of its unmanned, high maneuverability, mass deployment [3, 4], etc. As a new type of carrier in ocean engineering, UUV technology has important strategic significance in the development of marine resources and enhancement of marine military power [5, 6].

With the deepening of ocean development layer by layer, single UUV is difficult to meet the demand of executing complex and diversified missions with wide coverage due to its limited functional load and control range capability, prompting the transition of UUV application research towards multi-UUV formation control [7, 8]. Compared with a single UUV, UUV formation has stronger robustness, greater communication capability, greater flexibility, higher operational efficiency, and wider operational range [9]. Multi-UUV formation technology improves the execution efficiency in the fields of underwater search and rescue, environmental detection, surveillance and reconnaissance, and gaming and roundup [10]. At the same time, it can perform complex tasks that cannot be accomplished by traditional manned platforms, such as all-around, long-cycle, unmanned, and systematic defense alerts offshore and target sea area cleaning and reconnaissance. In complex

Received 31 May 2024; Accepted 18 December 2024; Published 15 February 2025. This paper was recommended for publication in its revised form by editorial board member, Jinwen Hu.
Email Address: *yanzheping@hrbeu.edu.cn
*Corresponding author.

marine environments, model parameter perturbations and external disturbances are huge obstacles to formation control [11−13]. At the same time, since the main means of underwater communication for multi-UUV formation is hydroacoustic communication, it has weak communication characteristics, such as a large propagation delay and susceptibility to communication interruption. The study of formation control methods applicable to weak communication conditions is important for enhancing the reliability, redundancy, and robustness of the formation system.

As a current research hotspot, UUV technology has been widely researched by researchers from various countries, from mission planning to platform control, but there are tricky challenges in multi-UUV formation control. Currently, frequent formation control algorithms include the leader-following method [14], artificial potential field method [15], reinforcement learning [16], and virtual structure method [17]. Multi-UUV formation requires collaborative execution of ocean missions according to the expected formation. Reliable communication between UUVs is crucial for the stable control of formation systems, and sampling mechanisms can reduce the communication frequency and better meet the needs of the formation system. The sampling methods applied in multi-agent systems can be divided into synchronous sampling and asynchronous sampling. In marine environments, due to limited technology, the synchronization of samplers cannot be achieved between UUVs, increasing the practicality of asynchronous sampling. Ding and Zheng [18] proposed an asynchronous sampling tracking protocol that guarantees bounded tracking error via the Lyapunov-Krasovskii method and designed a consistent controller gain matrix to achieve the formation tracking of heterogeneous nonlinear multi-agent system. For the networked mobile robot formation problem with communication delays, Peng *et al.* [19] solved the asynchronous clock formation problem by detecting the timing of synchronization points and combining the temporal and sequential characteristics of the messages to ensure that the messages have the correct order at the receiver. Han and Zeng [20] designed an asynchronous pulse mechanism that solves asymmetric feedback saturation by the convex hull method to enable the precise convergence of the system with communication delays. To improve control performance and decrease the energy consumption of a second-order multi-agent system, Yang *et al.* [51] proposed a distributed asynchronous control protocol, which reduces the interaction frequency and improves the formation consistency. Zhang and Su designed a distributed discrete observer using relative sampling output information and solved the asynchronous consensus problem for a multi-intelligent body system under switching topology by asynchronous sampling data distributed output feedback control [47]. Asynchronous sampling improves the control efficiency, but it takes up more computational resources and increases the number of communications between intelligences.

In practical applications, unnecessary information interactions occur when the formation system is close to stabilization, leading to energy waste in the formation system. Significantly reducing communication and computational energy consumption while ensuring the formation control performance of multi-intelligent body systems is the key to improving system stability. The event-triggered method is an important technique for reducing control energy consumption in intelligent agent cooperative control, controlling the necessary interactions and computations of members in the formation [21]. To address the problem of multi-surface ship formation under the influence of model parameter perturbation and current disturbance, Zheng *et al.* [13] designed a dynamic event triggering mechanism, and proposed a model parameter-free formation controller by combining sliding mode control and adaptive control. Song *et al.* [22] introduced internal dynamic variables into the trigger function, and combined the adaptive method and the minimum learning parameter method to design a multi-unmanned vessel formation controller based on edge event triggering under the influence of current disturbances. For the formation control problem of fractional-order multi-agent system, Meng *et al.* [23] proposed a dynamic event triggering SMC controller, designed a dynamic triggering mechanism using combined measurement vectors, and dynamically adjusted the threshold parameters of the triggering condition through auxiliary variables. Xia *et al.* [24] proposed an activatable dynamic event-triggered protocol, designed an event-triggered detector and a controller by combining adaptive control, and demonstrated the effectiveness of this approach with multi-spacecraft formation control. Yu *et al.* [25] proposed an event triggering mechanism based on position and direction and designed a high-gain extended state observer combined with a backstepping method, which reduces the requirement for velocity information and realizes the distributed formation control of multi-ground vehicles. Ma *et al.* [48] designed an event-triggered fault-tolerant formation controller based on the framework of the backtracking method in finite time to realize the formation control of multiple UAVs under external perturbations and flight faults.

Although the event-triggered mechanism effectively reduces the communication frequency, it requires real-time measurement of the system state. The continuous computation of the event-triggered mechanism will cause excessive resource loss, in order to solve this problem [26], the self-triggered control is proposed, which predicts the next triggering moment based on the information of the system at the current triggering moment [27]. For the second-order multi-agent system affine formation problem, Ma *et al.* [28] designed an event-triggered proportional-integral controller based on sampled data and combined with the self-triggered control, which effectively reduces the frequency of information interactions and controller computations. Zhao *et al.* [29] designed an interval observer and an event-triggered state compensator, and obtained the local triggering time through a self-triggering controller to achieve formation containment control of heterogeneous multi-agent system with external perturbations and missing state quantities [30]. For the problem of multi-spacecraft attitude synchronization with time-varying communication delay, Xie *et al.* [31] established a formation attitude dynamics model, proposed a dynamic event formation control strategy combined with a nonlinear observer, and designed a self-triggering function based on the triggering information, which avoids the continuous calculation of event triggering. Chai *et al.* [32] designed a self-triggering control scheme based on an observer, which reduces communication energy consumption while ensuring formation error and state estimation error, and achieves formation control of multi-intelligent body without directional topology. Jin *et al.* [33] designed a dual closed-loop self-triggering control framework considering unknown wind perturbation, which realized stable flight of a fixed-wing UAV formation under speed and overload constraints, while avoiding continuous rapid sampling. Zhao *et al.* [49] designed a self-triggered approximate optimal neural control method for nonlinear systems based on ADP, which obtains the update time of the next control strategy through the self-triggering mechanism and avoids the continuous monitoring of the system state by hardware devices.

Distributed model predictive control (DMPC) deals with multi-constraint control problems through rolling optimization and feedback correction, and achieves accurate control through prediction [34, 35]. With the development of DMPC in multi-agent formation control, triggered MPC enters into the limelight. To address the consistency problem of linear discrete MAS, Zhan *et al.* [36] weighed the control inputs and triggering intervals and designed a distributed self-triggered MPC method to realize the dynamic consensus of multi-agents. Mi *et al.* [37] designed a DMPC cooperative controller for dynamically decoupled agent systems based on a self-triggering mechanism, which guarantees the control performance and reduces the communication load at the same time. For multi-constrained linear time-invariant systems with disturbances, Kolarijani *et al.* [38] proposed a sampling strategy based on set theory and designed a robust formation MPC control algorithm to achieve constraint tightening. Zou *et al.* [39] designed a dynamic triggering mechanism based on the information of neighboring nodes, which balances resource consumption and control performance, and realizes asynchronous coordinated predictive control of multi-agent under perturbations. Wei *et al.* [40] obtained the next triggering time by solving local optimization problems and proposed a self-triggering min-max DMPC control algorithm to achieve nonlinear MAS formation control under communication delay and disturbance influence. Yang *et al.* [50] constructed a robust constraint set based on the estimation information of a discrete nonlinear perturbation observer and designed a self-triggered distributed MPC controller combined with an adaptive prediction mechanism to realize the cooperative control of a nonlinear system under perturbation and systematic constraints. So far, DMPC has not been applied to multi-UUV formation control with communication delays, and there are two shortcomings in related studies on triggered DMPC: one is that the control object has a simple nonlinear model or only kinematic models have been used; the other is that the effects of communication delays, time-varying disturbances, and model parameter perturbations on the formation control were not simultaneously considered.

To solve the aforementioned issues and enable the triggered DMPC to be applied to the multi-UUV formation control with multiple constraints, nonlinearity and strong coupling in complex environments, as well as to improve the efficiency of solving the communication delay problem, this paper proposes a DRMPC formation controller based on a dual closed-loop structure and self-triggering mechanism, which reduces information redundancy while enabling the multi-UUV system to maintain the target formation and accurately track the target trajectory under model parameter perturbations and ocean current disturbances. The main contributions of the paper are summarized as follows:

(1) A self-triggered DRMPC formation controller is proposed for the first time to address the multi-UUV 3D formation problem under bounded time-varying communication delay and multiple constraints. This controller realizes asynchronous communication among formation members, reduces the communication load, and reduces the information redundancy.
(2) The RMPC and FESO in the inner-loop controller work together to solve the problem of bounded disturbances and model parameter perturbations affecting the formation control and improve the robustness of the system.
(3) The stability and feasibility of the self-triggered formation controller at the triggering moment are analyzed by using the input-to-state practical stable (ISpS) theorem and mathematical induction, which provides a new idea for DMPC to handle multi-constraint, nonlinear multi-agent collaborative control under time-varying communication delays.

The remainder of the paper is organized as follows: Section 2 establishes the UUV mathematical model and provides important lemmas and problem description. Section 3 provides a detailed introduction to the design and theoretical analysis of a self-triggered formation controller. Section 4 verifies the effectiveness of the self-triggered formation controller through simulation experiments. Section 5 briefly summarizes the paper and suggests future research directions.

Notations: $\mathbb{N}_{[m,n]}$ denotes a positive integer within $[m, n]$, $I_n \in \mathbb{R}^{n\times n}$ denotes the identity matrix, $\mathbf{0}_{n\times m}$ denotes the $n \times m$-dimensional zero matrix, and $c(\cdot)$, $s(\cdot)$ and $t(\cdot)$ denote the cosine, sine and tangent functions, respectively. assuming $v \in \mathbb{R}^n$, $\mu^{\alpha}(v) = \text{sign}(v)|v|^{\alpha}$, and sign$(\cdot)$ denotes the sign function.¡

2. Preliminaries

2.1. *UUV mathematical model*

The UUV studied in the paper is a three-dimensional flat structure that can be approximated as left-right symmetric with large damping in the transverse roll direction; therefore, motion in the transverse roll direction is usually ignored when designing controllers [41]. To study the motion law of UUV, we selected the inertial coordinate system $O_E X_E Y_E Z_E$ and the body-fixed coordinate system $O_B X_B Y_B Z_B$ to describe the motion of UUV, and the schematic diagram of the coordinate systems is shown in Fig. 1. Usually, $\eta = [x; y; z; \theta; \psi]$ is used to describe the position and attitude of the UUV in the inertial coordinate system, and $\nu = [u; v; w; q; r]$ is used to describe the velocity and angular velocity of the UUV in the body-fixed coordinate system. The UUV is controlled by the actuator that generates force and torque to control its motion, and the control input vector is $\tau = [\tau_u; \tau_v; \tau_w; \tau_q; \tau_r]$.

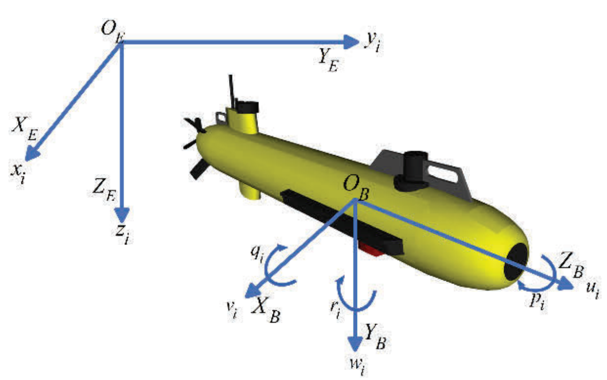

Fig. 1. UUV coordinate system.

Taking UUV_i as an example, its system model is Eq. (1):

$$\begin{aligned} \dot{\eta}_i &= J_i(\eta_i)\nu_i = f_1(\eta_i, \nu_i) \\ \dot{\nu}_i &= M_i^{-1}[\tau_i - C_i(\nu_i)\nu_i - D_i(\nu_i)\nu_i - g_i(\eta_i)] = f_2(\nu_i, \tau_i) \end{aligned}, \quad (1)$$

where M_i and $C_i(\nu_i)$ are the inertia and Coriolis centripetal matrices containing the hydrodynamic added mass, respectively, and $D_i(\nu_i)$ is the hydrodynamic damping coefficient matrix. $g_i(\eta_i)$ is the restoring force and moment, which is assumed to cancel each other since gravity and buoyancy are acting on the same line, and hence $g_i(\eta_i) = \mathbf{0}$. $J_i(\eta_i)$ is the rotation matrix, i.e.,

$$J_i(\eta_i) = \begin{bmatrix} c(\theta)c(\psi) & -s(\psi) & s(\theta)c(\psi) & \\ c(\theta)s(\psi) & c(\psi) & s(\theta)s(\psi) & \mathbf{0}_{3\times 2} \\ -s(\theta) & 0 & c(\theta) & \\ & \mathbf{0}_{2\times 3} & 1 & 0 \\ & & 0 & 1/c(\theta) \end{bmatrix}. \quad (2)$$

2.2. *Problem formulation*

The information interaction between UUVs is represented by a directed graph $G = (\mathcal{V}, \mathcal{E}, \mathcal{W})$ containing n nodes, and each UUV in the formation corresponds to a node in the directed graph G, where $\mathcal{V} = \{1, 2, \ldots, n\}$, $\mathcal{E} = \{\varepsilon_{ij} : i, j \in \mathcal{V}, i \neq j\} \subseteq \mathcal{V} \times \mathcal{V}$, and $\mathcal{W} = [w_{ij}] \in \mathrm{R}^{n\times n}$ are the vertex set, edge set, and adjacency matrix of the directed graph G, respectively. The set of adjacent individuals of UUV_i is $\mathcal{N}_i = \{j : \varepsilon_{ji} \in \mathcal{E}\}$, and the cardinality of set $\mathcal{N}_i$ is n_i. In the adjacency matrix, when $\varepsilon_{ji} \in \mathcal{E}$, $w_{ij} = 1$, i.e., UUV_i can receive the information sent by UUV_j; otherwise, $w_{ij} = 0$, which means that UUV_i cannot receive the information from UUV_j [42].

Under the directed graph, this paper investigates the multi-UUV formation tracking problem, aiming to design an asynchronous self-triggered controller so that the positions and velocities of all UUVs reach a relatively stable state under the influence of communication delays, bounded disturbances, and model parameter perturbations. The formation control objective is defined as follows:

$$\lim_{t_k^i\to\infty}\{\eta_{i0}(t_k^i)\} = \lim_{t_k^i\to\infty}\{\eta_i(t_k^i) - \eta_0(t_k^i) - \Delta_i\} = 0, \quad \forall i \in \mathbb{N}_{[1,n]}, \quad (3)$$

$$\lim_{t_k^i\to\infty}\{\eta_{ij}(t_k^i)\} = \lim_{t_k^i\to\infty}\{\eta_i(t_k^i) - \eta_j(t_k^i) - \Delta_{ij}\} = 0, \quad \forall i, j \in \mathbb{N}_{[1,n]}, \quad (4)$$

$$\lim_{t_k^i\to\infty}\{\nu_{ij}(t_k^i)\} = \lim_{t_k^i\to\infty}\{\nu_i(t_k^i) - \nu_j(t_k^i)\} = 0, \quad \forall i, j \in \mathbb{N}_{[1,n]}, \quad (5)$$

where $\eta_i(t_k^i)$ and $\nu_i(t_k^i)$ are the position and velocity of UUV_i at moment t_k^i, respectively; $\eta_0(t_k^i)$ is the position of virtual leader UUV_0 at moment t_k^i; Δ_i is the target distance between UUV_i and UUV_0; and Δ_{ij} is the target distance between UUV_i and UUV_j.

2.3. *Important lemmas*

Lemma 1 ([40]). *For a system $x(t_k^i+1)=f(x(t_k^i),u(t_k^i))$ with a robust invariant set, there exists a positive definite function $V(\cdot):\mathbb{R}^n\to\mathbb{R}$ satisfying $\alpha_1(\|x\|)\le V(x)\le\alpha_2(\|x\|)+c_1$ and $V(f(x,u))-V(x)\le-\alpha_3(\|x\|)+\gamma(\|w\|)+c_2$, where c_1 and c_2 are positive real numbers, $\alpha_1(\cdot)$, $\alpha_2(\cdot)$, and $\alpha_3(\cdot)$ are $\mathcal{K}_\infty$ functions, and $\gamma(\cdot)$ is an $\mathcal{K}$ function; then, the system is input-to-state practically stable (ISpS) in the robust invariant set.*

Lemma 2 ([43]). *For a perturbed system $x(t_k^i+1)=f(x(t_k^i),d(t_k^i))$, if $f(x(t_k^i),d(t_k^i))\in\Omega$, for any $x\in\Omega$ and $d(t_k^i)\in\Xi$, then the set Ω is the robust invariant set of the system.*

Lemma 3 ([43]). *For a discrete system $x(t_k^i+1)=f(x(t_k^i),u(t_k^i),d(t_k^i))$, $\Xi_N(\Omega)$ is said to be a robust N-step set of sets Ω if for any $x(t_k^i)\in\Xi_N(\Omega)\subset\mathbb{R}^n$ and $d(t_k^i)\in\mathbb{W}$, there exists a feasible sequence of control inputs $U_N=\{u(0|t_k^i),\dots,u(N-1|t_k^i)\}$ such that $x(N|t_k^i)\in\Omega$, subject to control input and state constraints, i.e. $\Xi_N(\Omega)=\{x(t_k^i)\in\Omega|\exists U_N:x(N|t_k^i)\in\Omega,\forall d(t_k^i)\in\mathbb{W}\}$.*

3. Controller Design

In this section, an asynchronous communication strategy with communication delay is proposed, and an extended state observer and RMPC are designed to resist the effects of model parameter perturbations and current disturbances. Then, a self-triggered distributed formation controller with a dual closed-loop structure is proposed, and the control structure diagram is shown in Fig. 2. Finally, the formation controller is theoretically analyzed.

3.1. *Asynchronous communication strategy*

First, we design the asynchronous communication strategy under communication delay, and Fig. 3 is a schematic diagram of asynchronous communication. t_k^i is the triggering moment of intermittent communication of UUV_i, at which UUV_i receives the prediction information from neighboring UUVs, and calculates the optimal communication interval and the new control inputs. τ_k^{ij} is the communication delay when UUV_j sends information to UUV_i. If $\exists i,j\in\mathcal{N}, i\ne j$, and t_k^i, t_k^j are not equal and independent of each other, the formation system communicates asynchronously, and the UUVs cannot update their states simultaneously.

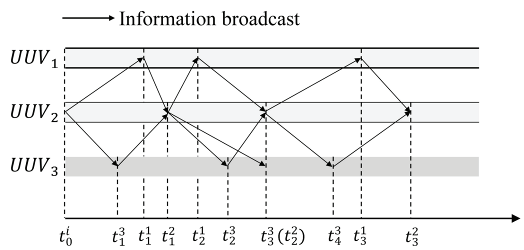

Fig. 3. Asynchronous communication schematic.

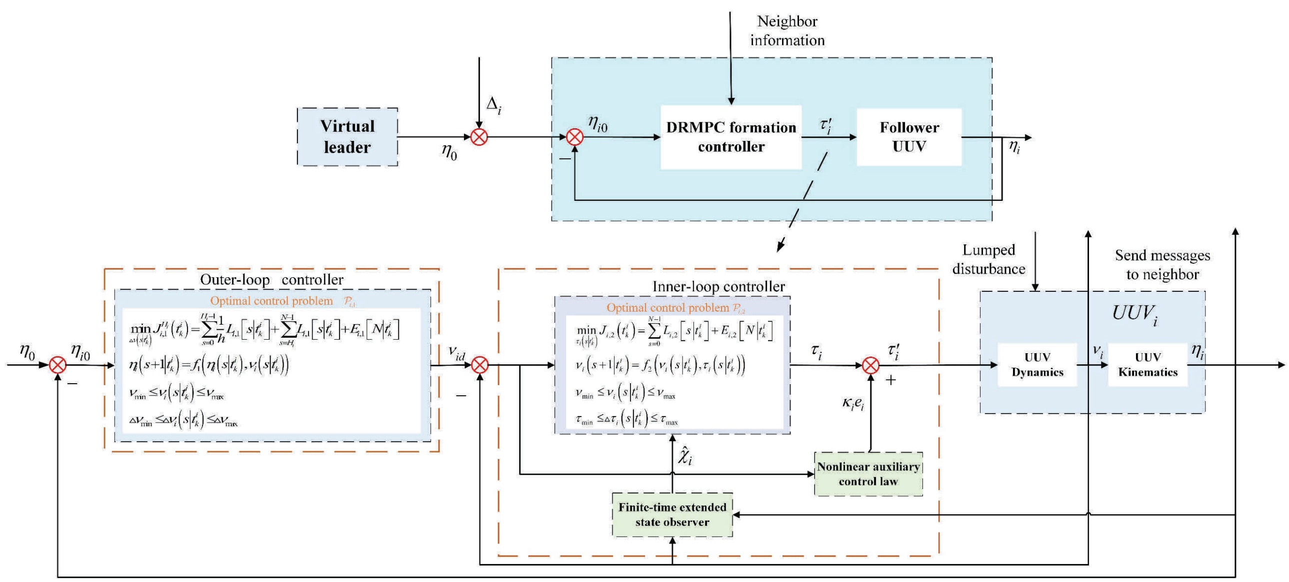

Fig. 2. Block diagram of the formation controller.

Assumption 1. When the control interval and the communication delay are large, UUVs cannot receive new information for a long time, thereby causing instability in multi-UUV formation systems. Taking UUV_i as an example, the local sampling moment t_k^i and the communication delay τ_k^{ij} need to satisfy the following conditions[40]: (1) $T \le t_{k+1}^i - t_k^i \le H_{\max} \cdot T$; (2) $0 \le \tau_k^{ij} \le T_{\max} \cdot T$. where $H_{\max}$ and $T_{\max}$ are both integer multiples of the control period, which denote the maximal sampling interval and the maximal communication delay, respectively.

At moment t_k^i, the predicted state sequence broadcasted by UUV_i is $\boldsymbol{\eta}_i^b(t_k^i) = (\eta_i^b(0|t_k^i), \ldots, \eta_i^b(N-1|t_k^i))$, and its expression is:

$$\eta_i^b(s|t_k^i) = \begin{cases} \eta_i^*(s|t_k^i), & s \in \mathbb{N}_{[0,N-1]} \\ 0, & s \in \mathbb{N}_{[N,\hbar)} \end{cases}, \tag{6}$$

where $\eta_i^b(s|t_k^i)$ denotes the optimal prediction state. The predicted velocity sequence for UUV_i broadcasting is $\boldsymbol{\nu}_i^b(t_k^i) = (\nu_i^b(0|t_k^i), \ldots, \nu_i^b(N-1|t_k^i))$, and its expression is:

$$\nu_i^b(s|t_k^i) = \begin{cases} \nu_i^*(s|t_k^i), & s \in \mathbb{N}_{[0,N-1]} \\ 0, & s \in \mathbb{N}_{[N,\infty)} \end{cases}, \tag{7}$$

where $\nu_i^*(s|t_k^i)$ denotes the optimal prediction velocity. Assuming that $\boldsymbol{\eta}_j^b(t_k^{ij})$ and $\boldsymbol{\nu}_j^b(t_k^{ij})$ are the latest state prediction information and velocity prediction information sent by UUV_j to UUV_i at moment t_k^{ij}, respectively, $t_k^{ij} = \max\{t_l^j \in \mathbb{N} | t_l^j < t_k^i\}$, we can categorize them into the following two scenarios according to the different communication delays:

(1) When $0 \le \tau_k^{ij} \le t_k^i - t_k^{ij}$, UUV_i can receive the latest information from UUV_j at moment t_k^i.
(2) When $t_k^i - t_k^{ij} < \tau_k^{ij} \le T_{\max} \cdot T$, UUV_i cannot receive the latest information from UUV_j at moment t_k^i, so UUV_i can only use the information $\boldsymbol{\eta}_j^b(t_{k-1}^{ij})$ and $\boldsymbol{\nu}_j^b(t_{k-1}^{ij})$ received at the previous moment.

Thus, the predictive information $\boldsymbol{\eta}_j(t_k^i)$ and $\boldsymbol{\nu}_j(t_k^i)$ of the neighboring UUV_j used by UUV_i in the subsequent local optimization problem can be constructed as

$$\begin{aligned} \boldsymbol{\eta}_j(t_k^i) &= (\eta_j^b(0|t_k^i), \eta_j^b(1|t_k^i), \ldots, \eta_j^b(N-1|t_k^i)) \\ \boldsymbol{\nu}_j(t_k^i) &= (\nu_j^b(0|t_k^i), \nu_j^b(1|t_k^i), \ldots, \nu_j^b(N-1|t_k^i)) \end{aligned}, \tag{8}$$

$$\eta_j^b(s|t_k^i) = \begin{cases} \eta_j^*(s|t_k^i), & s \in \mathbb{N}_{[0,N-1]} \\ 0, & s \in \mathbb{N}_{[N,\bar{H}+N+T_{\max}]} \end{cases}, \tag{9}$$

$$\nu_j^b(s|t_k^i) = \begin{cases} \nu_j^*(s|t_k^i), & s \in \mathbb{N}_{[0,N-1]} \\ 0, & s \in \mathbb{N}_{[N,\bar{H}+N+T_{\max}]} \end{cases}. \tag{10}$$

3.2. *FESO design*

First, we give an auxiliary variable $\omega_i = J_i \nu_i$ and transform the model (1) to obtain a new UUV model:

$$\begin{aligned} \dot{\eta}_i &= \omega_i \\ \dot{\omega}_i &= J_i M_i^{-1} \tau_i - J_i M_i^{-1} J_i h(\omega_i) \omega_i + \mathcal{X}_i \end{aligned}. \tag{11}$$

Assumption 2. Define the function $h(\omega)\omega = [C(\omega) + D(\omega)]\omega$. Since the actuator of the UUV has certain physical constraints that limit the motion of the UUV, there exists a coefficient μ such that $\|h(\omega)\omega\| \le \mu \|\omega\|^2$[41].

where $\mathcal{X}_i = J_i S_i \nu_i + \delta_i$ is the set total perturbation, δ_i denotes the model parameter perturbation, and the matrix S_i is:

$$S_i = \begin{bmatrix} 0 & -r_i & q_i & & \\ r_i & 0 & r_i \mathrm{t}(\theta_i) & \mathbf{0}_{3\times 2} & \\ -q_i & -r_i \mathrm{t}(\theta_i) & 0 & & \\ & \mathbf{0}_{2\times 3} & 0 & 0 & \\ & & 0 & q_i \mathrm{t}(\theta_i) & \end{bmatrix}. \tag{12}$$

Assumption 3. The set total uncertainty $\mathcal{X}_i$ in Eq. (11) is bounded and continuously differentiable, its derivative is bounded, i.e., $\|\dot{\mathcal{X}}_i\| \le \bar{\mathcal{X}}$, and $\bar{\mathcal{X}}$ is a positive constant [44].

In this section, an FESO is designed to estimate the uncertainty of the UUV system at a fixed time. $\hat{\eta}_i$, $\hat{\omega}_i$, and $\hat{\mathcal{X}}_i$ are defined as the estimates of η_i, ω_i, and $\mathcal{X}_i$, and the estimation errors are defined as $\boldsymbol{e}_{i1} = \hat{\eta}_i - \eta_i$, $\boldsymbol{e}_{i2} = \hat{\omega}_i - \omega_i$, and $\boldsymbol{e}_{i3} = \hat{\mathcal{X}}_i - \mathcal{X}_i$. The designed FESO is:

$$\begin{aligned} \dot{\hat{\eta}}_i &= \hat{\omega}_i - b_{i1}(\mathrm{sig}^{a_{i1}}(\boldsymbol{e}_{i1}) + \boldsymbol{e}_{i1}) \\ \dot{\hat{\omega}}_i &= \hat{\mathcal{X}}_i - J_i M_i^{-1} h(\hat{\omega}_i)\hat{\omega}_i + J_i M_i^{-1}\tau_i - b_{i2}(\mathrm{sig}^{a_{i2}}(\boldsymbol{e}_{i2}) \\ &\quad + \rho_i \boldsymbol{e}_{i1}) \\ \dot{\hat{\mathcal{X}}}_i &= -b_{i3}(\mathrm{sig}^{a_{i3}}(\boldsymbol{e}_{i3}) + \rho_i \boldsymbol{e}_{i1}) \end{aligned}, \tag{13}$$

where $\rho_i = |\boldsymbol{e}_{i1}|^{a_{i1}-1}$, the design parameters of the FESO are $a_{i1} \in (0.67, 1)$, $a_{i2} = 2a_{i1} - 1$, $a_{i3} = 3a_{i1} - 2$, b_{i1}, b_{i2}, and b_{i3} are positive.

Theorem 1. *For system* (11), *if the assumptions hold, the estimation error converges to the origin in finite time, i.e.,* $\hat{\eta}_i \equiv \eta_i$, $\hat{\omega}_i \equiv \omega_i$, *and* $\hat{\mathcal{X}}_i \equiv \mathcal{X}_i$. *Therefore, compensation for model parameter perturbations can be achieved by* $\hat{\mathcal{X}}_i$.

Proof. Derive the estimation error:

$$\begin{aligned}\dot{\boldsymbol{e}}_{i1} &= \boldsymbol{e}_{i2} - b_{i1}(\mathrm{sig}^{a_{i1}}(\boldsymbol{e}_{i1}) + \boldsymbol{e}_{i1}) \\ \dot{\boldsymbol{e}}_{i2} &= \boldsymbol{e}_{i3} - J_i M_i^{-1} J_i(h(\hat{\omega}_i)\hat{\omega}_i - h(\omega_i)\omega_i) - b_{i2}(\mathrm{sig}^{a_{i2}} \\ &\quad \times (\boldsymbol{e}_{i1}) + \rho_i \boldsymbol{e}_{i1}) \\ \dot{\boldsymbol{e}}_{i3} &= -b_{i3}(\mathrm{sig}^{a_{i3}}(\boldsymbol{e}_{i1}) + \rho_i \boldsymbol{e}_{i1}) - \dot{\mathcal{X}}_i\end{aligned} . \quad (14)$$

We introduce the auxiliary variable $\Gamma_i = [\mathrm{sig}^{a_{i1}}(\boldsymbol{e}_{i1}) + \boldsymbol{e}_{i1}; \boldsymbol{e}_{i2}; \boldsymbol{e}_{i3}]$. Theorem 1 holds if the auxiliary variable Γ_i converges to zero in finite time. We take the derivative of variable Γ_i

$$\begin{aligned}\dot{\Gamma}_i &= \begin{bmatrix} a_{i1}|\boldsymbol{e}_{i1}|^{a_{i1}-1}\dot{\boldsymbol{e}}_{i1} + \dot{\boldsymbol{e}}_{i1} \\ \dot{\boldsymbol{e}}_{i2} \\ \dot{\boldsymbol{e}}_{i3} \end{bmatrix} \\ &= \begin{bmatrix} a_{i1}|\boldsymbol{e}_{i1}|^{a_{i1}-1}[\boldsymbol{e}_{i2} - b_{i1}(\mathrm{sig}^{a_{i1}}(\boldsymbol{e}_{i1}) + \boldsymbol{e}_{i1})] \\ 0.5[\boldsymbol{e}_{i3} - b_{i2}(\mathrm{sig}^{a_{i2}}(\boldsymbol{e}_{i1}) + \rho_i \boldsymbol{e}_{i1})] \\ -0.5 b_{i3}(\mathrm{sig}^{a_{i3}}(\boldsymbol{e}_{i1}) + \rho_i \boldsymbol{e}_{i1}) \end{bmatrix} + \begin{bmatrix} 0_{5\times1} \\ 0_{5\times1} \\ -\dot{\mathcal{X}}_i^{\mathrm{T}} \end{bmatrix} \\ &\quad + \begin{bmatrix} \boldsymbol{e}_{i2} - b_{i1}(\mathrm{sig}^{a_{i1}}(\boldsymbol{e}_{i1}) + \boldsymbol{e}_{i1}) \\ 0.5[\boldsymbol{e}_{i3} - b_{i2}(\mathrm{sig}^{a_{i2}}(\boldsymbol{e}_{i1}) + \rho_i \boldsymbol{e}_{i1})] \\ -0.5 b_{i3}(\mathrm{sig}^{a_{i3}}(\boldsymbol{e}_{i1}) + \rho_i \boldsymbol{e}_{i1}) \end{bmatrix} + \begin{bmatrix} 0_{5\times1} \\ \mathrm{V}h_i^{\mathrm{T}} \\ 0_{5\times1} \end{bmatrix} \\ &= \mathrm{diag}\{l_i, l_i, l_i\} \begin{bmatrix} -a_{i1}b_{i1}I_5 & a_{i1}I_5 & 0 \\ -0.5 b_{i2}I_5 & 0 & 0.5\rho_i^{-1}I_5 \\ -0.5 b_{i3}\rho_i I_5 & 0 & 0 \end{bmatrix} \Gamma_i \\ &\quad + \begin{bmatrix} -b_{i1}I_5 & I_5 & 0 \\ -0.5 b_{i2}\rho_i I_5 & 0 & 0.5 I_5 \\ -0.5 b_{i3}\rho_i I_5 & 0 & 0 \end{bmatrix} \Gamma_i + G_{i3} + G_{i4} \\ &= \mathrm{diag}\{l_i, l_i, l_i\} G_{i1}\Gamma_i + G_{i2}\Gamma_i + G_{i3} + G_{i4},\end{aligned} \quad (15)$$

where $\Delta h_i = J_i M_i^{-1} J_i[h(\omega_i)\omega_i - h(\hat{\omega}_i)\hat{\omega}_i] = J_i M_i^{-1} J_i[h(\omega_i)\boldsymbol{e}_{i2} - h(\boldsymbol{e}_{i2})(\omega_i + \boldsymbol{e}_{i2})]$, $l_i = |\boldsymbol{e}_{i1}^{\mathrm{T}}|^{a_{i1}-1}$. The stability condition of Eq. (15) can be obtained through the Routh–Hurwitz criterion as $b_{i3} < 2b_{i1}b_{i2}$. □

We construct a Lyapunov function $V_i(e) = \Gamma_i^{\mathrm{T}} P_i \Gamma_i$ with P_i as a positive definite symmetric matrix satisfying Eq. (16).

$$\begin{aligned} G_{i1}^{\mathrm{T}} P_i + P_i G_{i1}^{\mathrm{T}} = -Q_1 \\ G_{i2}^{\mathrm{T}} P_i + P_i G_{i2}^{\mathrm{T}} = -Q_2 \end{aligned}, \quad (16)$$

where Q_1 and $Q_2$are positive definite symmetric Hermitian matrices. The remaining proof procedure can be found in our existing research results [41]. Taking the derivation of the function $V_i(e)$ and using Lemma 1 in the literature [41] can prove that the function $V_i(e)$ converges in a fixed time, thereby obtaining stable convergence of estimation errors. For the solution of the fixed time, we can also refer to our existing research results [41], and we will not analyze them in detail here.

3.3. *Self-triggered formation controller*

The formation controller adopts a dual closed-loop structure, which can guarantee the convergence of the tracking error while satisfying the attitude, velocity and control input constraints. The UUV discrete model (17) can be obtained by using the forward Euler method with Eq. (1).

$$\begin{aligned}\eta_i(s+1|t_k^i) &= \eta_i(s|t_k^i) + J_i(s|t_k^i)\nu_i(s|t_k^i)T \\ &= f_1(\eta_i(s|t_k^i), \nu_i(s|t_k^i)) \\ \nu_i(s+1|t_k^i) &= [I - M_i^{-1}(C_i + D_i)T]\nu_i(s|t_k^i) + M_i^{-1}T\tau_i(s|t_k^i) \\ &= A_i\nu_i(s|t_k^i) + B_i\tau_i(s|t_k^i) = f_2(\nu_i(s|t_k^i), \tau_i(s|t_k^i))\end{aligned} . \quad (17)$$

The outer-loop controller takes the amount of velocity change as input, which can control the velocity to change smoothly and suppress the effect caused by saturation control. The cost function of the outer-loop control problem of UUV_i at moment t_k^i is

$$\begin{aligned} J_{i,N}^{H_i}(t_k^i) &= J_{i,N}^{H_i}(\eta_i(t_k^i), \eta_{-i}(t_k^i), \Delta\nu_i(t_k^i)) \\ &= \sum_{s=0}^{H_i-1}\frac{1}{\hbar}L_{i,1}[s|t_k^i] + \sum_{s=H_i}^{N-1}L_{i,1}[s|t_k^i] + E_{i,1}[N|t_k^i], \end{aligned} \quad (18)$$

where $L_{i,1}[s|t_k^i] = \|\eta_{i0}(s|t_k^i)\|_{Q_1}^2 + \|\Delta\nu_i(s|t_k^i)\|_{R_1}^2 + \sum_{j\in\mathcal{N}_i}\|\eta_{ij}(s|t_k^i)\|_{Q_1'}^2$ denotes the local generation value and $E_{i,1}[N|t_k^i] = \|\eta_{i0}(N|t_k^i)\|_{P_1}^2$ is the terminal generation value. $\Delta\nu_i(t_k^i) = \nu_i(t_k^i) - \nu_i(t_k^i - 1)$ is the velocity variation, $\boldsymbol{\eta}_{-i}(t_k^i) = (\boldsymbol{\eta}_{i_1}(t_k^i), \ldots, \boldsymbol{\eta}_{i_{n_i}}(t_k^i))$ is the predicted state information of adjacent UUVs, $i_{n_i} \in \mathcal{N}_i$, and $\Delta\boldsymbol{\nu}_i(t_k^i)$ is the sequence of velocity variations. Q_1, Q_1', R_1, and P_1 are the weighting matrices. H_i is the triggering interval, which is a single control period when $H_i(t_k^i) = 1$. The parameter $\hbar \geq 1$ adjusts the control performance and the percentage of communication load, the larger the parameter $\hbar$, the more the system values communication load, and vice versa, the more it values the control performance. We achieve the self-triggered decision of intermittent communication by the outer-loop controller, whose control problem $\mathcal{P}_{i,1}$ at the moment t_k^i is designed as

$$\begin{aligned} &\min_{\Delta\nu_i(s|t_k^i)} \left\{ \begin{array}{l} J_{i,1}^{H_i}(\eta_i(t_k^i), \boldsymbol{\eta}_{-i}(t_k^i), \Delta\boldsymbol{\nu}_i(t_k^i)) \\ \text{such that } \eta_i(H_i|t_k^i) \in \Xi_{N-H_i}(\Omega_{i1}) \end{array} \right\} \\ &\text{s.t. } \eta_i(s+1|t_k^i) = f_1(\eta_i(s|t_k^i), \nu_i(s|t_k^i)) \\ &\eta_i(0|t_k^i) = \eta_i(t_k^i) \\ &-\nu_{\max} \leq \nu_i(s|t_k^i) \leq \nu_{\max} \\ &-\nu_{\max} \leq \Delta\nu_i(s|t_k^i) \leq \Delta\nu_{\max} \\ &\Omega_{i1} = \{\eta_i(s|t_k^i) | \|\eta_{i0}(s|t_k^i)\|_{P_1}^2 \leq \sigma_{i1}\}, \sigma_{i1} \in \mathbb{R}^+ \end{aligned} , \quad (19)$$

where $\nu_{\max}$ and $\Delta\nu_{\max}$ are the constraint values for velocity and velocity increment, Ω_{i1} is the terminal set and $\Xi_{N-H_i}(\Omega_i)$ is the $N-H_i$-step robust set of UUV_i. Define the optimal value of this control problem $\mathcal{P}_{i,1}$ at the trigger interval H_i is $V_{i,N}^{H_i}(\eta_i(t_k^i),\boldsymbol{\eta}_{-i}(t_k^i))$. We design the self-triggering method to determine the optimal triggering interval H_i^* at moment t_k^i, which satisfies the relation $t_{k+1}^i = t_k^i + H_i^*$. H_i^* is calculated as follows:

$$H_i^* = \max\{H_i \in \mathbb{N}_{[1,\bar{H}]} | V_{i,N}^{H_i}(t_k^i) \le V_{i,N}^1(t_k^i)\}. \tag{20}$$

The velocity increment sequence $\Delta\boldsymbol{\nu}_i^*(t_k^i)$ corresponding to the optimal triggering interval H_i^* is taken as the optimal solution sequence to the control problem $\mathcal{P}_{i,1}$ at the moment t_k^i, and then the optimal velocity sequence $\boldsymbol{\nu}_i^*(t_k^i)$ is obtained, which is taken as the expectation value of the inner-loop controller. The inner-loop controller will be solved H_i^* times within the triggering interval, and the cost function of its inner-loop control problem is:

$$\begin{aligned} J_{i,N}(t_k^i) &= J_{i,N}(\nu_i(t_k^i),\boldsymbol{\nu}_{-i}(t_k^i),\tau_i(t_k^i)) \\ &= \sum_{s=0}^{N-1} L_{i,2}[s|t_k^i] + E_{i,2}[N|t_k^i], \end{aligned} \tag{21}$$

where $L_{i,2}[s|t_k^i] = \|\nu_{id}(s|t_k^i)\|_{Q_2}^2 + \|\tau_i(s|t_k^i)\|_{R_2}^2 + \sum_{j\in\mathcal{N}_i}\|\nu_{ij}(s|t_k^i)\|_{Q_2'}^2$ denotes the local generation value and $E_{i,2}[N|t_k^i] = \|\nu_{id}(N|t_k^i)\|_{P_2}^2$ is the terminal generation value. $\boldsymbol{\tau}_i(t_k^i)$ is the control input sequence, and $\boldsymbol{\nu}_{-i}(t_k^i) = (\boldsymbol{\nu}_{i_1}(t_k^i),\ldots,\boldsymbol{\nu}_{i_{n_i}}(t_k^i))$ is the predicted velocity information of adjacent UUVs. Q_2, Q_2', R_2, and P_2 are the weighting matrices.

The inner-loop control problem $\mathcal{P}_{i,2}$ at moment t_k^i is designed as follows:

$$\begin{aligned} &\min_{\bar{\tau}_i(s|t_k^i)} \{J_{i,N}(\boldsymbol{\nu}_i(t_k^i),\boldsymbol{\nu}_{-i}(t_k^i),\boldsymbol{\tau}_i(t_k^i))\} \\ &\text{s.t. } \nu_i(s+1|t_k^i) = f_2(\nu_i(s|t_k^i),\tau_i(s|t_k^i)) \\ &\nu_i(0|t_k^i) = \nu_i(t_k^i) \\ &-\nu_{\max} \le \nu_i(s|t_k^i) \le \nu_{\max} \\ &-\tau_{\max} \le \tau_i(s|t_k^i) \le \tau_{\max} \\ &\Omega_{i2} = \{\nu_i(s|t_k^i) | \|\nu_{id}(s|t_k^i)\|_{P_2}^2 \le \sigma_{i2}\}, \quad \sigma_{i2} \in \mathbb{R}^+ \end{aligned}, \tag{22}$$

where $\tau_{\max}$ is the constraint value of the control quantity and Ω_{i2} is the terminal set. Solving problem $\mathcal{P}_{i,2}$ yields the optimal control input $\boldsymbol{\tau}_i^*(t_k^i)$ for the nominal system, which is ideally unaffected by perturbations. In the motion of UUV, the control input τ_i' that actually drives the UUV contains the control input τ_i of the nominal system and the auxiliary control law $\kappa_i e_i$, $e_i = \nu_i - \nu_i'$. Solving the Riccati equation yields the coefficient κ_i.

$$\begin{aligned} &2A_i^{\mathrm{T}}P_iA_i + 2\kappa_i^{\mathrm{T}}B_i^{\mathrm{T}}P_iB_i\kappa_i - P_i + \rho + \kappa_i^{\mathrm{T}}B_i^{\mathrm{T}}P_iA_i \\ &\quad + A_i^{\mathrm{T}}P_iB_i\kappa_i = -Q_2, \end{aligned} \tag{23}$$

where $P_i = A_iA_i^{\mathrm{T}}$, the discrete model of an actual system with disturbances is as follows:

$$\nu_i'(s+1|t_k^i) = A_i\nu_i'(s|t_k^i) + B_i\tau_i'(s|t_k^i) + d_i(s|t_k^i). \tag{24}$$

Subtracting Eq. (17) and Eq. (24) yields an error model as

$$e_i(s+1|t_k^i) = A_ie_i(s|t_k^i) + B_i\kappa_ie_i(s|t_k^i) + d_i(s|t_k^i). \tag{25}$$

Assumption 4. The disturbance d_i satisfies the relationship $d_i^{\mathrm{T}}P_id_i \le \boldsymbol{e}_i^{\mathrm{T}}\rho\boldsymbol{e}_i$ [45].

Theorem 2. *When Assumption 4 holds, the velocity error e_i can gradually approach 0 through the control law κ_ie_i.*

Proof By constructing a Lyapunov function $\mathcal{F}_e = e_i^{\mathrm{T}}P_ie_i$, it can be shown that $\mathcal{F}_e \ge 0$. It is sufficient to show that $\mathcal{F}_e$ is a monotonically decreasing function to conclude that the velocity error e_i tends to 0. Expanding and simplifying $\Delta\mathcal{F}_e$ according to Assumption 4 and Lemma 1 [45] yields

$$\begin{aligned} \Delta\mathcal{F}_{e_i}(s+1|t_k^i) &= \mathcal{F}_{e_i}(s+1|t_k^i) - \mathcal{F}_{e_i}(s|t_k^i) \\ &\le e_i^{\mathrm{T}}(2A_i^{\mathrm{T}}P_iA_i + 2\kappa_i^{\mathrm{T}}B_i^{\mathrm{T}}P_iB_i\kappa_i - P_i + \rho \\ &\quad + \kappa_i^{\mathrm{T}}B_i^{\mathrm{T}}P_iA_i + A_i^{\mathrm{T}}P_iB_i\kappa_i)e_i \\ &\le -e_i^{\mathrm{T}}Q_2e_i < 0. \end{aligned} \tag{26}$$

As a result, the system error e_i will gradually converge to 0, and the nonlinear auxiliary control law can suppress the effect of the perturbation. □

3.4. *Theoretical analysis*

The cost function of the outer-loop control problem can be rewritten as

$$J_{i,N}^{H_i}(t_k^i) = \sum_{s=0}^{H_i-1}\frac{1}{\hbar}L_{i,1}[s|t_k^i] + V_{i,N-H_i}(\eta_i(t_k^i),\boldsymbol{\eta}_{-i}(t_k^i)), \tag{27}$$

$$\begin{aligned} &V_{i,l}(\eta_i(t_k^i),\boldsymbol{\eta}_{-i}(t_k^i)) \\ &= \min_{\nu_i(s|t_k^i)} \left\{ \begin{aligned} &L_{i,1}(\eta_i(s|t_k^i),\boldsymbol{\eta}_{-i}(s|t_k^i),\nu_i(s|t_k^i)) \\ &\quad + V_{i,l-1}(f_1(\eta_i(s|t_k^i),\nu_i(s|t_k^i)), \\ &\quad \times \boldsymbol{\eta}_{-i}(s+1|t_k^i)) \\ &\text{such that } \eta_i(s|t_k^i) \in \Xi_l(\Omega_{i1}), \\ &f(\eta_i(s|t_k^i),\nu_i(s|t_k^i)) \in \Xi_{l-1}(\Omega_{i1}) \end{aligned} \right\}. \end{aligned} \tag{28}$$

Assumption 5. For UUV_i, there exists a set of terminal constraints Ω_{i1} with terminal controllers $\mathcal{K}_i(\eta_i(t_k^i))$ [40], and there exists a $\mathcal{K}$-function $\sigma_i(\cdot)$ and a constant α, such that

$$\begin{aligned} &E_{i,1}(\eta_i(s+1|t_k^i)) - E_{i,1}(\eta_i(s|t_k^i)) \\ &\quad \le L_{i,1}(\eta_i(s|t_k^i), \eta_{-i}(s|t_k^i), \mathcal{K}_i) + \varpi_i, \end{aligned} \tag{29}$$

where $\varpi_i = \sigma_i(\|d_i(s)\|) + \alpha$.

Feasibility: Based on the mathematical induction method to prove the feasibility of the formation controller, assuming that for UUV_i, its control problem $\mathcal{P}_{i,1}$ has an optimal solution $\boldsymbol{\nu}_i^*(t_k^i) = (\nu_i^*(0|t_k^i), \ldots, \nu_i^*(N-1|t_k^i))$ satisfying the constraints at moment t_k^i, the candidate velocity sequence $\tilde{\nu}_i(t_{k+1}^i)$ at moment t_{k+1}^i can be constructed as follows:

$$\tilde{\nu}_i(s|t_{k+1}^i) = \begin{cases} \nu_i^*(s+H_i^*|t_k^i), & s \in \mathbb{N}_{[0,N-H_i^*-1]} \\ \mathcal{K}_i(\tilde{\eta}_i(s|t_k^i)), & s \in \mathbb{N}_{[N-H_i^*,N-1]} \end{cases}. \tag{30}$$

Its corresponding system state is $\tilde{\eta}_i(s+1|t_{k+1}^i) = f_1(\tilde{\eta}_i(s|t_{k+1}^i), \tilde{\nu}_i(s|t_{k+1}^i))$, where $\tilde{\eta}_i(0|t_{k+1}^i) = \tilde{\eta}_i(t_{k+1}^i)$, and it is known that $\tilde{\nu}_i(t_{k+1}^i)$ satisfies the constraint by Assumption 5 and $\boldsymbol{\nu}_i^*(t_k^i)$.

When $s \in \mathbb{N}_{[0,N-H_i^*]}$, the system states $\tilde{\eta}_i(s|t_{k+1}^i)$ satisfy the constraints.

When $s \in \mathbb{N}_{[N-H_i^*+1,N]}$, the system states remain in the set of constraints through the terminal controller $\mathcal{K}_i(\tilde{\eta}_i(s|t_{k+1}^i))$. Therefore, the system states all satisfy the constraints, proving the feasibility of this controller.

Stability: We prove the stability of this formation controller by proving that the function $V_{i,N}^{H_i^*}$ in the control problem $\mathcal{P}_{i,1}$ is the ISpS function.

The local cost function $L_{i,1}$ in Problem $\mathcal{P}_{i,1}$ is quadratic form, and Q_1, Q_1', and R_1 are positive definite matrices. It is known that there exists $\mathcal{K}_\infty$-function $\alpha_L(\|\eta_i(t_k^i)\|) = \underline{\lambda}(Q_1)\|\eta_i(t_k^i)\|^2$ such that $L_{i,1} \ge \alpha_L(\|\eta_i(t_k^i)\|)$, i.e., $V_{i,N}^{H_*^i} \ge \alpha_L(\|\eta_i(t_k^i)\|)$.

Based on these assumptions, it can be concluded that

$$\begin{aligned} &E_{i,1}(\eta_i(s+1|t_k^i)) - E_{i,1}(\eta_i(s|t_k^i)) \\ &\quad \le -L_{i,1}(\eta_i(s|t_k^i), \boldsymbol{\eta}_{-i}(s|t_k^i), \mathcal{K}_i(\eta_i(s|t_k^i))) + \varpi_i. \end{aligned} \tag{31}$$

Adding Eq. (31) from 0 to $N-1$ yields

$$\begin{aligned} &\sum_{s=0}^{N-1} L_{i,1}(\eta_i(s|t_k^i), \boldsymbol{\eta}_{-i}(s|t_k^i), \mathcal{K}_i(\eta_i(s|t_k^i))) \\ &\quad + E_{i,1}(\eta_i(N|t_k^i)) \le E_{i,1}(\eta_i(t_k^i)) + N\varpi_i, \end{aligned} \tag{32}$$

where $E_{i,1}(\eta_i(t_k^i)) = E_{i,1}(\eta_i(0|t_k^i))$; when Eq. (20) holds, $V_{i,N}^{H_i^*} \le V_{i,N}^1$.

Expression for the function $E_{i,1}$ yields the existence of a $\mathcal{K}_\infty$-function $\alpha_E(\|\eta_i(t_k^i)\|) = \bar{\lambda}(P_1)\|\eta_i(t_k^i)\|^2$ such that $E_{i,1}(\eta_i(t_k^i)) \le \alpha_E(\|\eta_i(t_k^i)\|)$, i.e. $V_{i,N}^{H_i^*} \le V_{i,N}^1 \le V_{i,N} \le \alpha_E(\|\eta_i(t_k^i)\|) + N\varpi_i$.

From Eqs. (18) and (27), we obtain

$$\begin{aligned} &J_{i,N-H_i^*}(\eta_i(t_{k+1}^i), \eta_{-i}(t_{k+1}^i), \nu_i^*(t_k^i)) \\ &\quad = J_{i,N}^{H_i^*}(\eta_i(t_k^i), \boldsymbol{\eta}_{-i}(t_k^i), \nu_i^*(t_k^i)) \\ &\qquad - \frac{1}{\hbar}\sum_{s=0}^{H_i^*-1} L_{i,1}(\eta_i(s|t_k^i), \boldsymbol{\eta}_{-i}(s|t_k^i), \nu_i^*(s|t_k^i)) \\ &\quad \le J_{i,N}^{H_i^*}(\eta_i(t_k^i), \boldsymbol{\eta}_{-i}(t_k^i), \nu_i^*(t_k^i)) - \frac{H_i^*}{\hbar}\alpha_L(\|\eta_i(t_k^i)\|), \end{aligned} \tag{33}$$

where the optimal velocity sequence is $\boldsymbol{\nu}_{i,N-H_i^*}^*(t_k^i) = (\nu_i^*(H_i^*|t_k^i), \ldots, \nu_i^*(N-1|t_k^i))$.

The state $\eta_i(t_{k+1}^i)$ of UUV_i can enter the terminal set under the action of a feasible solution, which follows from inequality (33) and Assumption 5:

$$\begin{aligned} &J_{i,N}(\tilde{\eta}_i(t_{k+1}^i), \boldsymbol{\eta}_{-i}(t_{k+1}^i), \tilde{\nu}_i(t_{k+1}^i)) \\ &\quad \le J_{i,N}^{H_i^*}(\eta_i(t_k^i), \boldsymbol{\eta}_{-i}(t_k^i), \nu_i^*(t_k^i)) - \frac{H_i^*}{\hbar}\alpha_L(\|\eta_i(t_k^i)\|) \\ &\qquad + H_i^*\varpi_i. \end{aligned} \tag{34}$$

When $t_k^i - t_k^{ij} < \tau_k^{ij} \le T_{\max} \cdot T$, the predicted state information of the neighbors of UUV_i is $\boldsymbol{\eta}_{-i}(t_{k+1}^i) = (\eta_{-i}(H_i^*|t_k^i), \ldots, \eta_{-i}(H_i^*+N-1|t_k^i))$.

Through the proof procedure in [46], it can be concluded that the relationship $V_{i,N}^1 \le V_{i,N}$.

$$\begin{aligned} V_{i,N}(\eta_i(t_k^i), \boldsymbol{\eta}_{-i}(t_k^i)) &= J_{i,N}(\eta_i(t_k^i), \eta_i(t_k^i), \nu_i^*(t_k^i)) \\ &= \sum_{s=0}^{N-1} L_{i,1}(\eta_i(s|t_k^i), \boldsymbol{\eta}_{-i}(s|t_k^i), \nu_i^*(s|t_k^i)) \\ &\quad + E_{i,1}(\eta_i^*(N|t_k^i)). \end{aligned} \tag{35}$$

This is obtained through the above inequality and Eq. (34):

$$\begin{aligned} &V_{i,N}^{H_i^*}(\eta_i(t_{k+1}^i), \boldsymbol{\eta}_{-i}(t_{k+1}^i)) \\ &\quad \le V_{i,N}^1(\eta_i(t_{k+1}^i), \boldsymbol{\eta}_{-i}(t_{k+1}^i)) \\ &\quad \le V_{i,N}(\eta_i(t_{k+1}^i), \boldsymbol{\eta}_{-i}(t_{k+1}^i)) \\ &\quad = J_{i,N}(\eta_i(t_{k+1}^i), \boldsymbol{\eta}_{-i}(t_{k+1}^i), \nu_i^*(t_{k+1}^i)) \\ &\quad \le J_{i,N}(\eta_i(t_{k+1}^i), \boldsymbol{\eta}_{-i}(t_{k+1}^i), \tilde{\nu}_i(t_{k+1}^i)) \\ &\quad \le J_{i,N}^{H_i^*}(\eta_i(t_k^i), \boldsymbol{\eta}_{-i}(t_k^i), \nu_i^*(t_k^i)) - \frac{H_i^*}{\hbar}\alpha_L(\|\eta_i(t_k^i)\|) \\ &\qquad + H_i^*\varpi_i \\ &\quad \le V_{i,N}^{H_i^*}(\eta_i(t_k^i), \boldsymbol{\eta}_{-i}(t_k^i)) - \frac{H_i^*}{\hbar}\alpha_L(\|\eta_i(t_k^i)\|) + H_i^*\varpi_i. \end{aligned} \tag{36}$$

When $0 \le \tau_k^{ij} \le t_k^i - t_k^{ij}$, new neighbor information $\boldsymbol{\eta}_{-i}(t_{k+1}^i) = (\eta_{-i}(0|t_{k+1}^i), \ldots, \eta_{-i}(N-1|t_{k+1}^i))$ will be used. Due to $\eta_i(\cdot|t_k^i)\mathbb{X}_i$, there exists a constant δ_i such that $\|\eta_i(\cdot|t_k^i)\| \le \delta_i$.

From the trigonometric inequality and the state constraints, the following relationship can be obtained:

When $s \in [0, N - H_i^* - 1]$, we obtain

$$\begin{aligned}&\|\eta_i(s|t_{k+1}^i) - \eta_j(s|t_{k+1}^i) - \Delta_{ij}\| \\ &\leq \|\eta_i(s|t_{k+1}^i) - \eta_j(H_i^* + s|t_k^i) - \Delta_{ij}\| \\ &\quad + \|\eta_j(s|t_{k+1}^i) - \eta_j(H_i^* + s|t_k^i)\| \\ &\leq \|\eta_i(s|t_{k+1}^i) - \eta_j(H_i^* + s|t_k^i) - \Delta_{ij}\| + 2\delta_i. \end{aligned} \tag{37}$$

Next, we consider $s \in [N - H_i^*, N - 1]$.

$$\begin{aligned}&\|\eta_i(s|t_{k+1}^i) - \eta_j(s|t_{k+1}^i) - \Delta_{ij}\| \\ &\leq \|\eta_i(s|t_{k+1}^i) - \Delta_{ij}\| + \|\eta_j(s|t_{k+1}^i)\| \leq \|\eta_i(s|t_{k+1}^i) \\ &\quad - \Delta_{ij}\| + \delta_i. \end{aligned} \tag{38}$$

The coupling term in the local cost function can be simplified by Eqs. (37) and (38):

$$\begin{aligned}&\sum_{s=0}^{N-1}\left(\sum_{j\in\mathcal{N}_i}\|\eta_{ij}(s|t_{k+1}^i)\|_{Q_1'}^2\right) \\ &= \sum_{s=0}^{N-1}\left(\sum_{j\in\mathcal{N}_i}\|\eta_i(s|t_{k+1}^i) - \eta_j(s|t_{k+1}^i) - \Delta_{ij}\|_{Q_1'}^2\right) \\ &\leq \sum_{s=0}^{N-H_i^*-1}\sum_{j\in\mathcal{N}_i}(\|\eta_i(s|t_{k+1}^i) - \eta_j(H_i^* + s|t_k^i) - \Delta_{ij}\|_{Q_1'} \\ &\quad + 2\delta_i)^2 + \sum_{s=N-H_i^*}^{N-1}\sum_{j\in\mathcal{N}_i}(\|\eta_i(s|t_{k+1}^i) - \Delta_{ij}\|_{Q_1'} + \delta_i)^2 \\ &\leq \sum_{s=0}^{N-1}\left(\sum_{j\in\mathcal{N}_i}\|\eta_i(s|t_{k+1}^i) - \eta_j(H_i^* + s|t_k^i) - \Delta_{ij}\|_{Q_1'}^2\right) \\ &\quad + H_i^*\bar{\lambda}(Q_1')\sum_{j\in\mathcal{N}_i}(3\delta_i^2 + 2\delta_i\Delta_{ij}) \\ &\quad + (N - H_i^*)\bar{\lambda}(Q_1')\sum_{j\in\mathcal{N}_i}(12\delta_i^2 + 4\delta_i\Delta_{ij}). \end{aligned} \tag{39}$$

Through Eq. (34) and the above inequality relation, we can obtain

$$\begin{aligned}&V_{i,N}^{H_*^i}(\eta_i(t_{k+1}^i), \hat{\boldsymbol{\eta}}_{-i}(t_{k+1}^i)) \leq V_{i,N}^1(\eta_i(t_{k+1}^i), \hat{\boldsymbol{\eta}}_{-i}(t_{k+1}^i)) \\ &\leq V_{i,N}(\eta_i(t_{k+1}^i), \hat{\boldsymbol{\eta}}_{-i}(t_{k+1}^i)) = J_{i,N}(\eta_i(t_{k+1}^i), \\ &\quad \times \hat{\boldsymbol{\eta}}_{-i}(t_{k+1}^i), \boldsymbol{\nu}_i^*(t_{k+1}^i)) \\ &\leq J_{i,N}(\eta_i(t_{k+1}^i), \hat{\boldsymbol{\eta}}_{-i}(t_{k+1}^i), \tilde{\nu}_i(t_{k+1}^i)) \leq J_{i,N}(\eta_i(t_{k+1}^i), \\ &\quad \times \boldsymbol{\eta}_{-i}(t_{k+1}^i), \tilde{\nu}_i(t_{k+1}^i)) + (N - H_i^*)\bar{\lambda}(Q_1')\sum_{j\in\mathcal{N}_i} \\ &\quad \times (12\delta_i^2 + 4\delta_i\Delta_{ij}) + H_i^*\bar{\lambda}(Q_1')\sum_{j\in\mathcal{N}_i}(3\delta_i^2 + 2\delta_i\Delta_{ij}) \\ &\leq J_{i,N}^{H_i^*}(\eta_i(t_k^i), \boldsymbol{\eta}_{-i}(t_k^i), \boldsymbol{\nu}_i^*(t_k^i)) - \frac{H_i^*}{\hbar}\alpha_L(\|\eta_i(t_k^i)\|) + \Theta_i \\ &\leq V_{i,N}^{H_i^*}(\eta_i(t_k^i), \boldsymbol{\eta}_{-i}(t_k^i)) - \frac{H_i^*}{\hbar}\alpha_L(\|\eta_i(t_k^i)\|) + \Theta_i, \end{aligned} \tag{40}$$

where $\Theta_i = (N - H_i^*)\bar{\lambda}(Q_1')\sum_{j\in\mathcal{N}_i}(12\delta_i^2 + 4\delta_i\Delta_{ij}) + H_i^*\bar{\lambda}(Q_1')\sum_{j\in\mathcal{N}_i}(3\delta_i^2 + 2\delta_i\Delta_{ij}) + H_i^*\varpi_i$.

Based on Lemma 1, we prove in detail that the function $V_{i,N}^{H_i^*}$ is an ISpS Lyapunov function, and the same applies for the inner-loop controller proof procedure.

4. Simulation Example

This section verifies the effectiveness and control performance of the proposed self-triggered formation controller through numerical experiments in two scenarios. The formation system consists of a virtual leader UUV and multiple following UUVs. Figure 4 shows the structure diagram of the target formation, with each following UUV maintaining a distance of 5 m from UUV_0 located at the center of the formation. Figure 5 shows the communication network diagram of the formation system, which is a directed spanning tree with UUV_0 as the root node. The detailed physical parameters of the UUV system selected in the experiment can be found in the literature [35].

The parameters in the numerical experiments are chosen as: $T = 0.2$ s, $N = 15T$, $H_{\max} = 5$, and $T_{\max} = 5$. The parameters of the formation controller are $Q_1 = \mathrm{diag}\{1, 3, 4, 6, 5\}$,

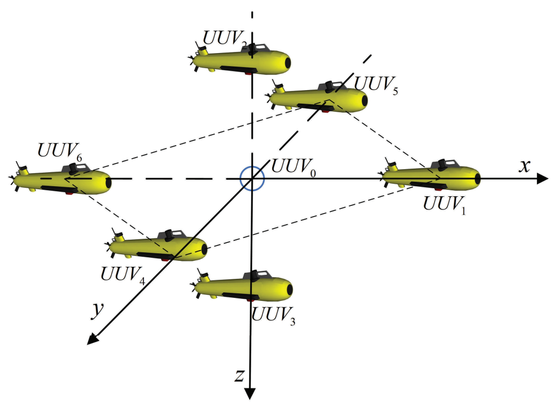

Fig. 4. Target formation structure chart.

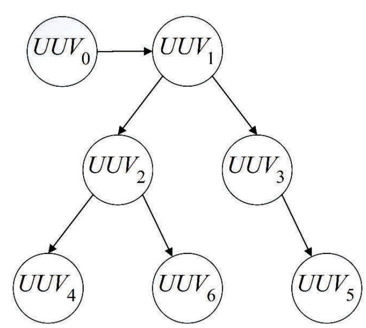

Fig. 5. Formation communication schematic.

$Q_1' = \mathrm{diag}\{1,1,1,1,1\}$, $R_1 = \mathrm{diag}\{8,8,8,2,2\}$, $Q_2 = \mathrm{diag}\{1,1,3,3,8\}$, $Q_2' = \mathrm{diag}\{1,1,1,1,1\}$, and $R_2 = \mathrm{diag}\{10^{-3},10^{-3},10^{-3},10^{-3},10^{-3}\}$. The velocity constraints are $\nu_{\max} = [2.5;0.6;0.6;\pi/18;\pi/9]$ and $\Delta\nu_{\max} = [0.1;0.08;0.08;\pi/36;\pi/18]$, and the control input constraints are $\tau_{\max} = [350;350;350;150;150]$. The parameters of the extended state observer are $a_{i1} = 0.85$, $b_{i1} = 0.4$, $b_{i2} = 0.2$, and $b_{i3} = 0.001$. The communication delay t_k^{ij} is an integer multiple of the control period T and varies randomly.

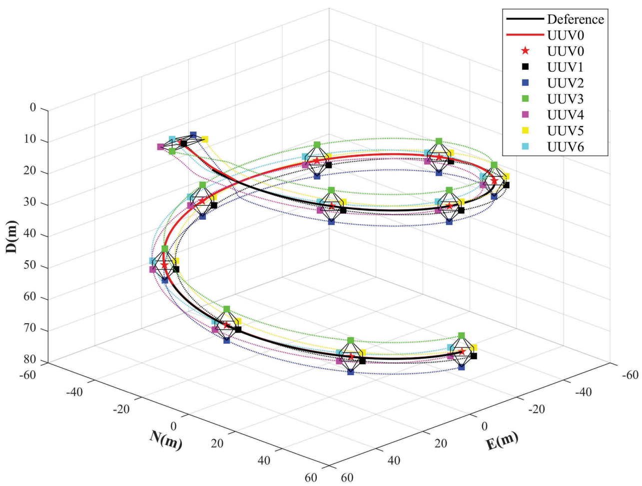

Fig. 6. UUV formation tracking trajectory.

The initial position of each UUV in the formation is on the water surface of $[-20,-5]\times[40,60]$, and the initial velocity is 0. The formation system needs to form and maintain the target formation during the movement, and the position deviations between each following UUV and the leader UUV are: $\Delta_1 = [5\ 0\ 0\ 0\ 0]$, $\Delta_2 = [0\ 0\ 5\ 0\ 0]$, $\Delta_3 = [0\ 0\ -5\ 0\ 0]$, $\Delta_4 = [0\ 5\ 0\ 0\ 0]$, $\Delta_5 = [0\ -5\ 0\ 0\ 0]$, and $\Delta_6 = [-5\ 0\ 0\ 0\ 0]$.

Simulation 1: Check the effectiveness and convergence performance of the proposed formation controller under the influence of time-varying communication delays. Each following UUV in the formation tracks the reference trajectory by maintaining the desired position deviation from the virtual UUV, and we choose the spiral diving curve as the reference trajectory of the virtual UUV with the following expression:

$$\begin{cases} x_0 = 50\sin(0.01\mathrm{t}) \\ y_0 = 50\cos(0.01\mathrm{t}), \quad \mathrm{t} \le 800\,. \\ z_0 = 5 + 0.075\mathrm{t} \end{cases} \tag{41}$$

Figures 6 and 7 depict the trajectory tracking effect and the position attitude change curve of the UUV formation system, respectively. It can be intuitively seen from the figures that the UUV formation starts from the water surface, forms the expected formation and tracks the reference

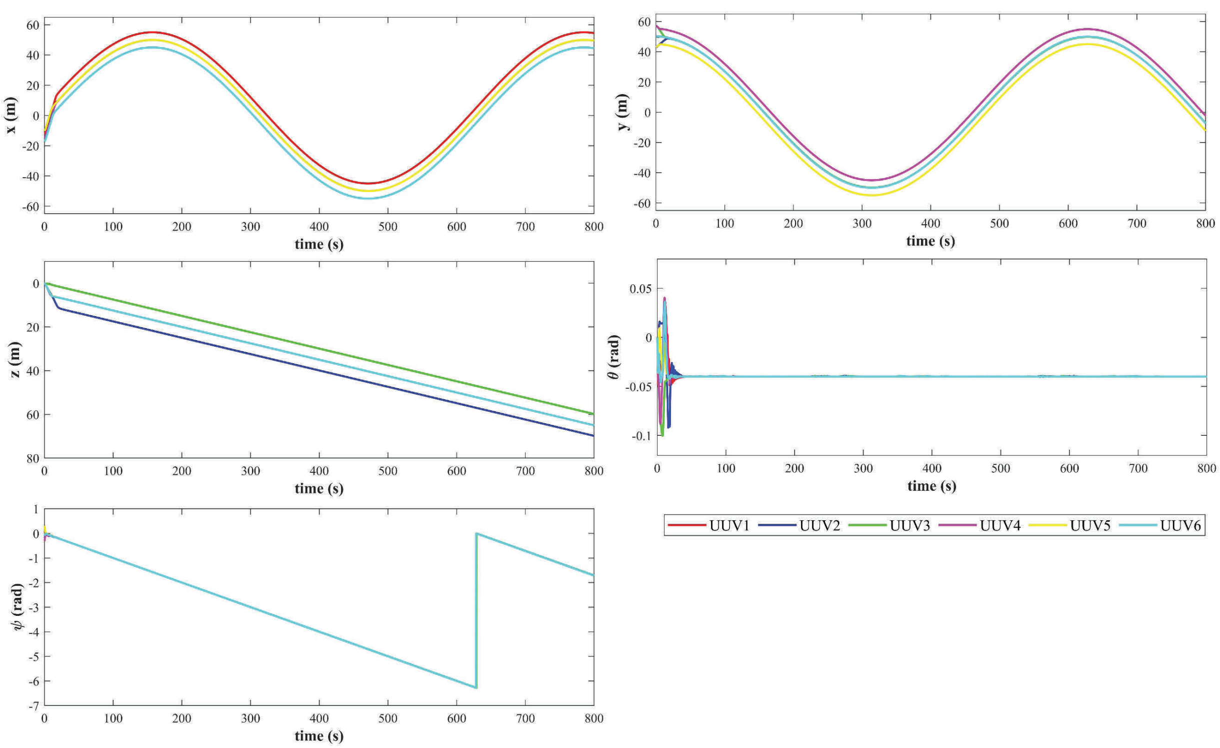

Fig. 7. UUV position and attitude change curve.

trajectory at 30 s, which indicates that the formation controller can effectively achieve the formation tracking task, and the attitude angle quickly converges to a stable state. Figures 8 and 9 show the velocity and control input plots over time, respectively, from which it can be seen that the formation system achieves stable convergence at approximately 30 s, and the velocity and control inputs remain stable after 30 s. Figure 10 depicts the tracking error variation curves for each UUV, and the tracking error rapidly converges within 30 s, and the error remains within 0.1 m. The experimental results verify that the self-triggered formation controller can effectively suppress the effect of communication delay on formation control, and quickly and accurately form the desired formation and track the reference trajectory.

Simulation 2: To better demonstrate the control performance of this self-triggered formation controller, the model parameter perturbation and bounded disturbance problems are considered in the second set of simulation experiments, where there is 15% uncertainty in the model parameters of the UUVs, and the bounded disturbance d_i is selected as

$$d_i(\mathrm{t}) = \begin{bmatrix} 0.25u_i^3 + 0.25\sin(0.05\mathrm{t}) \\ 0.3v_i^3 + 0.2\cos(0.05\mathrm{t}) \\ 0.15w_i^3 + 0.1\sin(0.05\mathrm{t} + \pi/4) \end{bmatrix}. \tag{42}$$

This group of simulation experiments simulates the UUV system to perform ocean missions, which requires the UUV to track the U-shaped route after completing the spiral diving. The reference trajectory of the virtual UUV is shown in Eqs. (43)–(46):

(1) Spiral diving curve

$$\begin{cases} x_0 = 50\sin(0.01\mathrm{t}) \\ y_0 = 50\cos(0.01\mathrm{t}), \quad \mathrm{t} \le 250\pi\,. \\ z_0 = 5 + 0.075\mathrm{t} \end{cases} \tag{43}$$

(2) U-shaped curve

$$\begin{cases} x_0 = 50 \\ y_0 = -0.5025(\mathrm{t} - 250\pi), \quad 250\pi < \mathrm{t} \le 250\pi + 200\,, \\ z_0 = 5 + 18.75\pi \end{cases} \tag{44}$$

$$\begin{cases} x_0 = 50\sin(0.01\mathrm{t} - 2\pi - 2) \\ y_0 = -100.5 + 50\cos(0.01\mathrm{t} - 2\pi - 2), \\ \qquad 250\pi + 200 < \mathrm{t} \le 350\pi + 200 \\ z_0 = 5 + 18.75\pi \end{cases}, \tag{45}$$

$$\begin{cases} x_0 = -50 \\ y_0 = -100.5 + 0.5025(\mathrm{t} - 350\pi - 200), \\ \qquad 350\pi + 200 < \mathrm{t} \le 350\pi + 400 \\ z_0 = 5 + 18.75\pi \end{cases}. \tag{46}$$

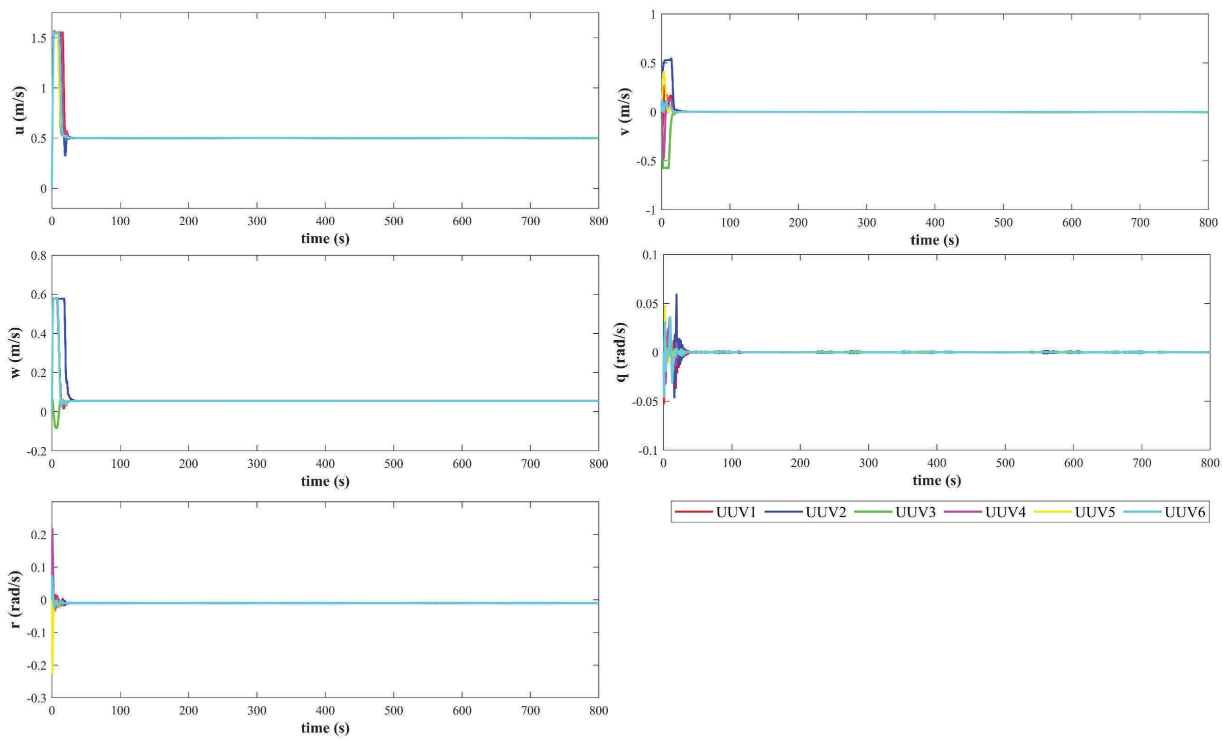

Fig. 8. UUV velocity change curve.

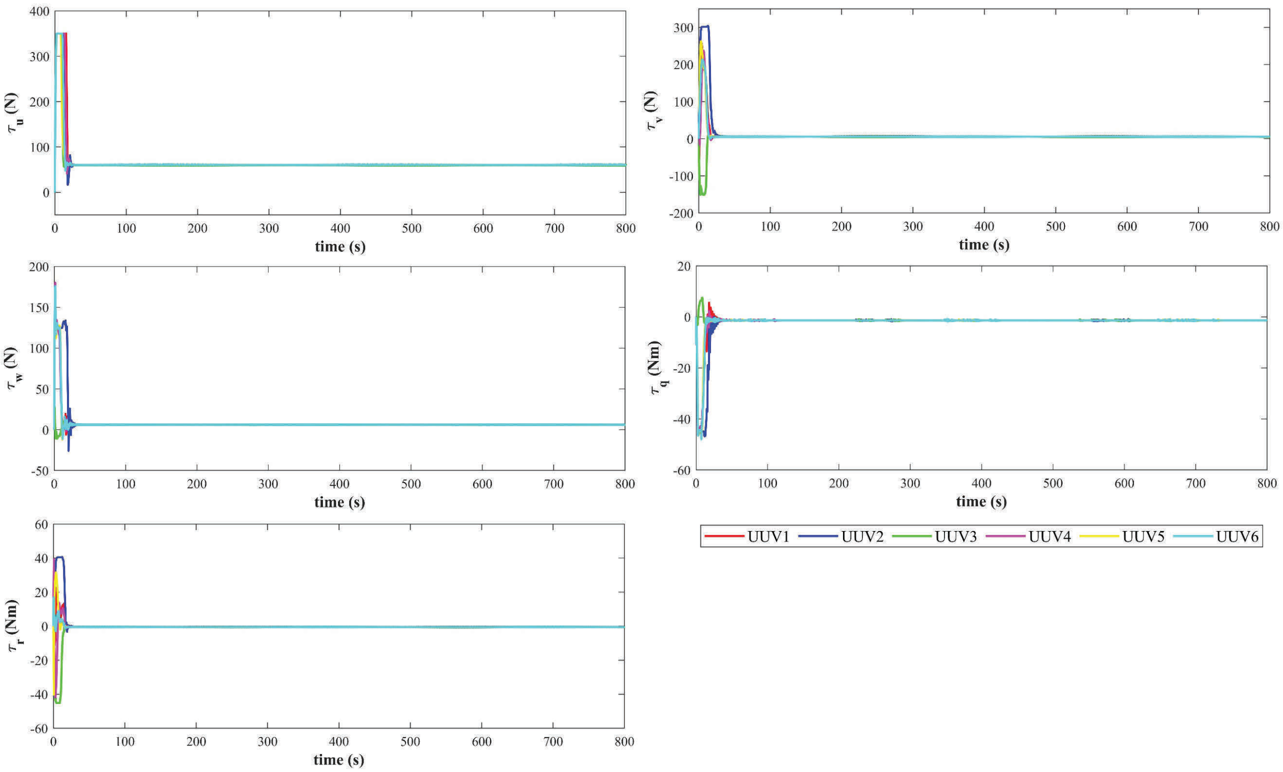

Fig. 9. UUV control input change curve.

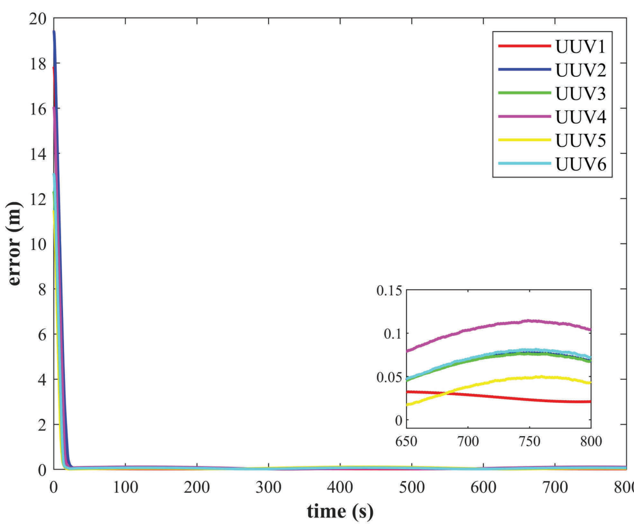

Fig. 10. Time-variation curve of formation tracking error.

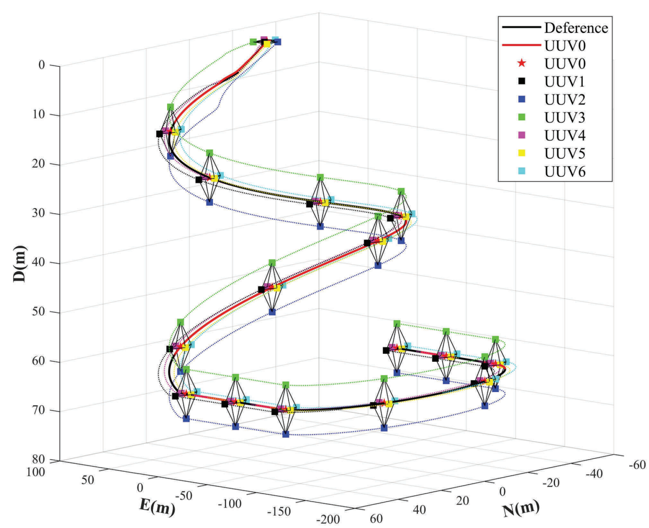

Fig. 11. UUV formation tracking trajectory.

The experimental results of the self-triggered formation controller in the complex environment are shown in Figs. 11–16. Figures 11 and 12 depict the trajectory and position attitude curve of the formation system over time. The figures demonstrate that the UUV system can quickly form a target formation and achieve smooth transitions between different routes, and accurately track the spiral diving curve and U-shaped route. Figures 13 and 14 show the velocity and control input over time graphs. The inner and outer loop control structure enhances the controllability of the system over the

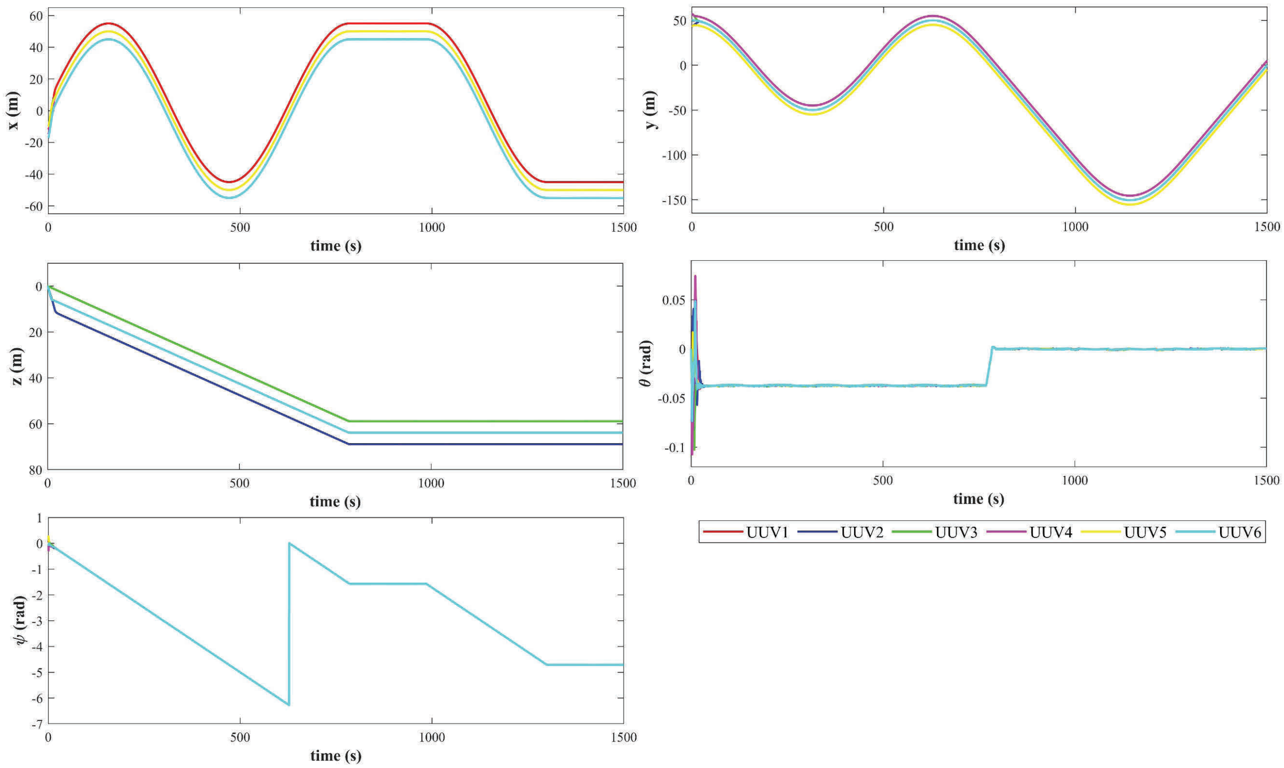

Fig. 12. UUV position and attitude change curve.

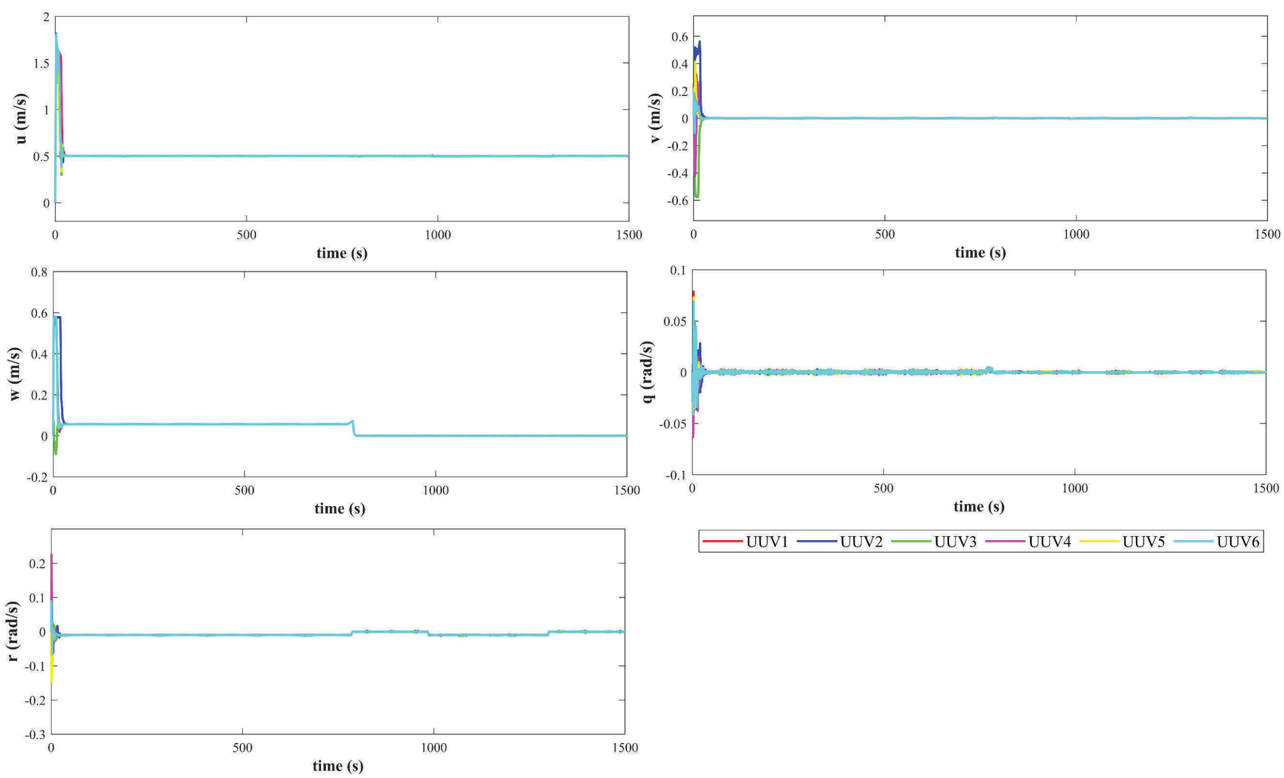

Fig. 13. UUV velocity change curve.

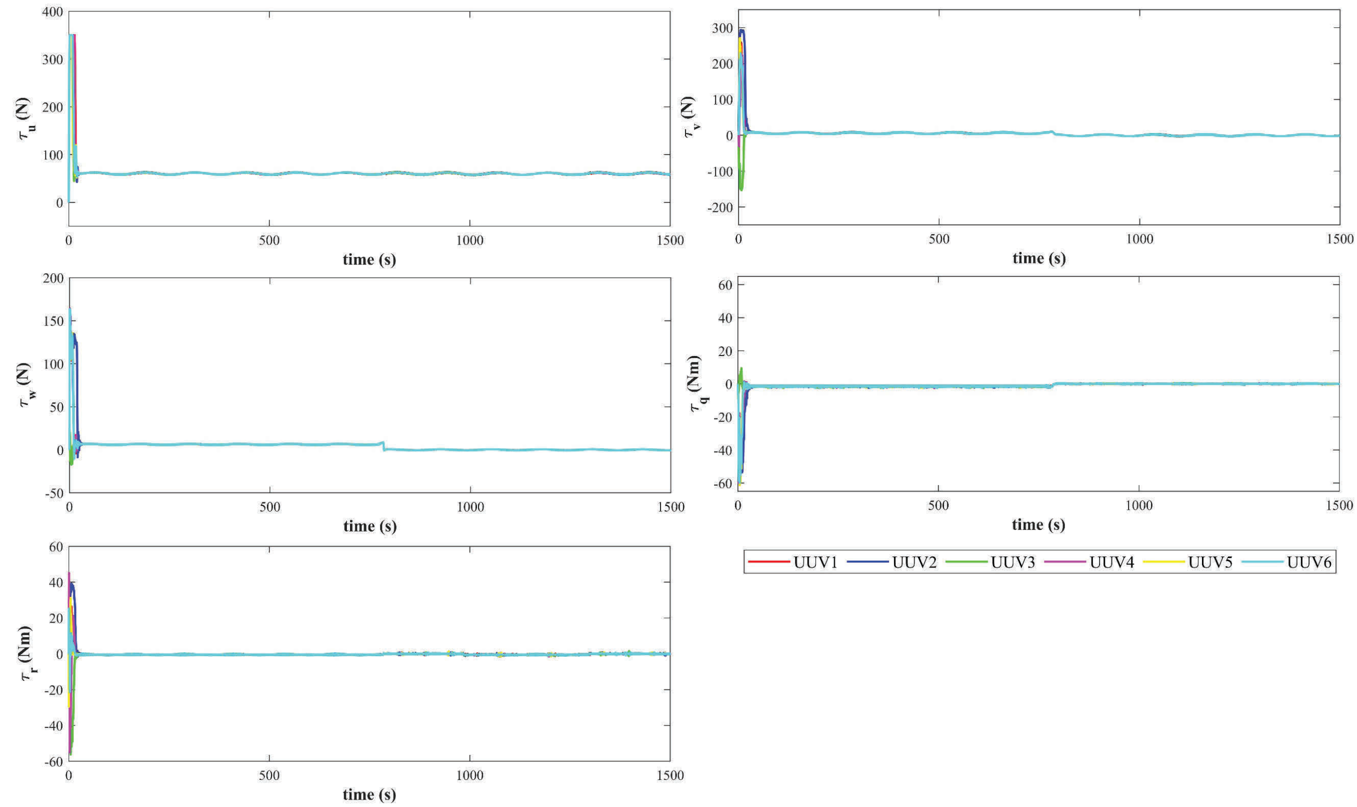

Fig. 14. UUV control input change curve.

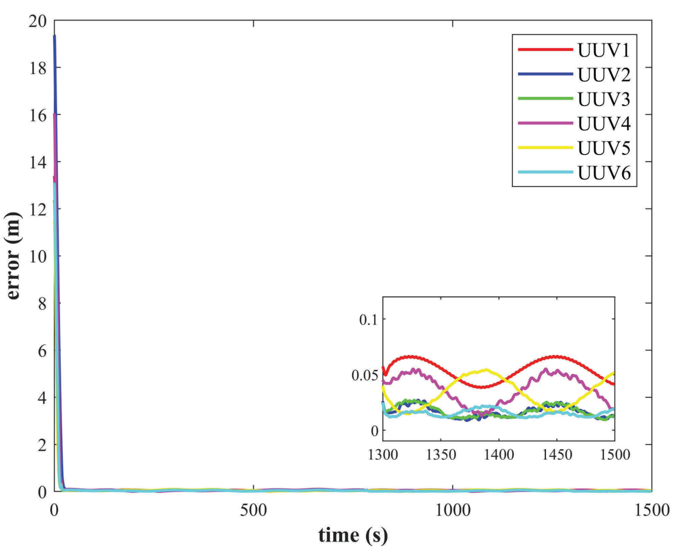

Fig. 15. Time-variation curve of formation tracking error.

velocity, and the auxiliary control law in the inner loop controller counteracts the influence of the sea current on the velocity by compensating for the control input, so the velocity can be kept constant. However, the control input may exhibit small fluctuations due to disturbances. Figure 15 shows the formation tracking error curve, which roughly shows that the tracking error converges within 30 s, and the error of all UUVs can be maintained within 0.07 m. Figure 16 shows the triggering situation of each UUV in 60–78 s, during which the formation system gradually converges to a stable state and the communication interval between UUVs will stabilize at 5 control cycles. Table 1 lists the number of communication triggers of each UUV during the motion process. If each control cycle is communicated, each UUV needs to communicate 7500 times, while the proposed self-triggered controller needs only approximately 1650 times. This can greatly relieve the communication load of the formation system, reduce the information redundancy, and improve the communication efficiency.

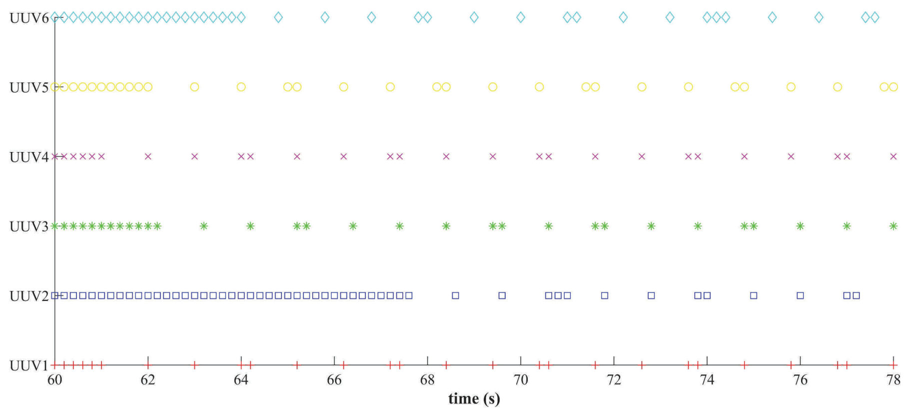

Fig. 16. 60–78 s for each UUV trigger moment.

Table 1. Communication frequency of each UUV.

	UUV1	UUV2	UUV3	UUV4	UUV5	UUV6
Periodic control	7500	7500	7500	7500	7500	7500
Self-triggered	1674	1638	1650	1623	1642	1645

5. Conclusion

In this paper, the formation control problem of a multi-UUV formation system under bounded communication delays under the influence of model parameter perturbations and external disturbances is investigated, and a self-triggered distributed robust model prediction controller with a dual closed-loop structure is proposed. The RMPC and FESO in the inner-loop controller work together to improve the stability of the system under model parameter perturbations and external disturbances. Based on the self-triggered mechanism, asynchronous communication between individual UUVs is realized, which reduces the communication load. Finally, the closed-loop stability and feasibility of this self-triggered formation controller are rigorously analyzed theoretically. Simulation experiments verify the effectiveness of this controller.

Considering the complexity and danger of the UUV working environment, obstacle avoidance during navigation is an unavoidable challenge, and the cooperative obstacle avoidance of UUV formation system and mission replanning after a failure of a formation member will be studied in future work.

Acknowledgments

This work was funded by the National Natural Science Foundation of China (No. 42327901, 52071102, 51679057, and 51609046), the Province Science Fund for Distinguished Young Scholars, China (No. J2016JQ0052).

ORCID

Jinyu Yan https://orcid.org/0000-0003-0889-2130

References

[1] H. Peng, B. Huang, M. J. Jin, C. Zhu and J. Y. Zhuang, Distributed finite-time bearing-based formation control for underactuated surface vessels with levant differentiator, *ISA Trans.* **147** (2024) 239–251.

[2] L. Zhang, Y. X. Zheng, Z. Y. Huang, B. Huang and Y. M. Su, Distributed global output-feedback formation control without velocity measurement for multiple unmanned surface vehicles, *ISA Trans.* **147**(2) (2024) 118–129.

[3] Y. Yang, Y. Xiao and T. S. Li, A survey of autonomous underwater vehicle formation: Performance, formation control, and communication capability, *IEEE Commun. Surv. Tutor.* **23**(2) (2021) 815–841.

[4] Z. P. Yan, J. Y. Yan, Y. F. Wu, S. J. Cai and H. X. Wang, A novel reinforcement learning based tuna swarm optimization algorithm for autonomous underwater vehicle path planning, *Math. Comput. Simulat.* **209** (2023) 55–86.

[5] J. Zhang, Z. X. Wang, G. J. Han, Y. J. Qian and Z. L. Li, A collaborative path planning method for heterogeneous autonomous marine vehicles, *IEEE Internet Things J.* **11**(1) (2023) 1465–1480.

[6] W. B. Zhao, Y. Q. Xia, D. H. Zhai and B. Cui, Adaptive event-triggered coordination control of unknown autonomous underwater vehicles under communication link faults, *Automatica* **158** (2023) 111277.

[7] Y. Y. Wang, W. X. Zhou, M. R. Fei and H. C. Yan, An unmanned surface vehicle for the launch and recovery of autonomous underwater vehicles: A novel design, *IEEE Robot. Autom. Mag.* **31**(1) (2024) 53–61.

[8] Y. Huang, X. Lin, M. Hernandez-Rocha, S. Narain, K. Pochiraju and B. Englot, Mission-oriented Gaussian process motion planning for UUVs over complex seafloor terrain and current flows, *IEEE Robot. Autom. Lett.* **9**(2) (2024) 1780–1787.

[9] W. Y. Cai, Z. Q. Liu, M. Y. Zhang, S. S. Lv and C. C. Wang, Cooperative formation control for multiple AUVs with intermittent underwater acoustic communication in IoUT, *IEEE Internet Things J.* **10**(17) (2023) 15301–15313.

[10] J. L. Du, J. Li and F. L. Lewis, Distributed 3D time-varying formation control of underactuated AUVs with communication delays based on data-driven state predictor, *IEEE Trans. Ind. Inform.* **19**(5) (2022) 6963–6971.

[11] Y. Lu, C. Y. Wen, T. L. Shen and W. D. Zhang, Bearing-based adaptive neural formation scaling control for autonomous surface vehicles with uncertainties and input saturation, *IEEE Trans. Neural Netw. Learn. Syst.* **32**(10) (2020) 4653–4664.

[12] D. J. Zhu and S. X. Yang, Current effect-eliminated optimal target assignment and motion planning for a multi-UUV system, *IEEE Trans. Intell. Transp. Syst.* **25**(8) (2024) 8419–8428.

[13] Y. X. Zheng, L. Zhang, B. Huang, C. Zhu and Y. M. Su, Dynamic event-triggered formation maneuver in cooperative marine surface vehicles control over directed communication networks, *Ocean Eng.* **281** (2023) 114622.

[14] M. Rani and N. Kumar, A neural network based efficient leader–follower formation control approach for multiple autonomous underwater vehicles, *Eng. Appl. Artif. Intell.* **122** (2023) 106102.

[15] W. Pang, D. Q. Zhu and C. Y. Sun, Multi-AUV formation reconfiguration obstacle avoidance algorithm based on affine transformation and improved artificial potential field under ocean currents disturbance, *IEEE Trans. Autom. Sci. Eng.* **21**(2) (2023) 1469–1487.

[16] B. Hadi, A. Khosravi and P. Sarhadi, Adaptive formation motion planning and control of autonomous underwater vehicles using deep reinforcement learning, *IEEE J. Ocean. Eng.* **49**(1) (2023) 311–328.

[17] Q. Z. Zhen, L. Wan, Y. L. Li and D. P. Jiang, Formation control of a multi-AUVs system based on virtual structure and artificial potential field on SE (3), *Ocean Eng.* **253** (2022) 111148.

[18] L. Ding and W. X. Zheng, Consensus tracking in heterogeneous nonlinear multi-agent networks with asynchronous sampled-data communication, *J. Syst. Control Lett.* **96** (2016) 151–157.

[19] L. Peng, F. Guan, L. Perneel, H. Fayyad-Kazan and M. Timmerman, Decentralized multi-robot formation control with communication delay and asynchronous clock, *J. Intell. Robot. Syst.* **89** (2018) 465–484.

[20] Y. Y. Han and Z. G. Zeng, Asynchronous impulsive protocols with asymmetric feedback saturation on leader-based formation control of multiagent systems, *IEEE Trans. Cybern.* **52**(9) (2020) 9931–9942.

[21] H. Y. Li and X. Li, Distributed model predictive consensus of heterogeneous time-varying multi-agent systems: With and without self-triggered mechanism, *IEEE Trans. Circuits Syst. I-Regul. Pap.* **67** (12) (2020) 5358–5368.

[22] S. Song, E. H. Zhang, W. K. Wang and T. Liu, Distributed dynamic edge-based event-triggered formation control for multiple underactuated unmanned surface vessels, *Ocean Eng.* **264** (2022) 112319.

[23] X. Meng, B. P. Jiang, H. R. Karimi and C. C. Gao, Leader–follower sliding mode formation control of fractional-order multi-agent systems: A dynamic event-triggered mechanism, *Neurocomputing* **557** (2023) 126691.

[24] L. N. Xia, Q. Li and R. Z. Song, Adaptive event-triggered average tracking control with activable event-triggering mechanisms, *IEEE Trans. Syst. Man Cybern. -Syst.* **53**(10) (2023) 6067–6079.

[25] K. T. Yu, Y. M. Li, Z. H. Peng and S. C. Tong, Distributed event-triggered formation control of planar vehicles without velocity sensors, *IEEE Trans. Veh. Technol.* **72**(3) (2022) 2988–3000.

[26] X. J. Song, Z. W. Fan, S. F. Lu, Y. L. Yan and B. Z. Yue, Predefined-time sliding mode attitude control for liquid-filled spacecraft with large amplitude sloshing, *Eur. J. Control.* **77** (2024) 100970.

[27] F. Q. Di, A. J. Li, Y. Guo, B. J. Liu and C. Q. Wang, Disturbance observer-based finite-time coordinated control for spacecraft formation flying with event-triggered communication, *Nonlinear Dyn.* **111**(15) (2023) 14213–14230.

[28] S. H. Ma, D. Zhang, Y. Zhao, C. X. Xian and Y. S. Zheng, Event-triggered affine formation maneuver control for second-order multi-agent systems with sampled data, *J. Frankl. Inst.-Eng. Appl. Math.* **360**(18) (2023) 14645–14659.

[29] Y. A. Zhao, F. L. Zhu and D. Z. Xu, Self-triggered bipartite formation-containment control for heterogeneous multi-agent systems with disturbances, *Neurocomputing.* **548** (2023) 126382.

[30] W. L. Yang, Z. Y. Shi and Y. S. Zhong, Robust time-varying formation control for uncertain multi-agent systems with communication delays and nonlinear couplings, *Int. J. Robust Nonlinear Control.* **34** (1) (2024) 147–166.

[31] X. Xie, T. Sheng and X. Q. Chen, Self-triggered formation control for multi-spacecraft attitude coordination with communication delays, *J. Frankl. Inst.-Eng. Appl. Math.* **360**(18) (2023) 14696–14711.

[32] X. F. Chai, J. Liu, Y. Yu and C. Y. Sun, Observer-based self-triggered control for time-varying formation of multi-agent systems, *Sci. China-Inf. Sci.* **64** (2021) 1–16.

[33] Z. H. Jin, L. S. Bai, Z. X. Wang and P. P. Zhang, Self-triggered distributed formation control of fixed-wing unmanned aerial vehicles subject to velocity and overload constraints, *IEEE Trans. Autom. Sci. Eng.* **21**(3) (2023) 4082–4093.

[34] A. Capannolo, G. Zanotti, M. Lavagna and G. Cataldo, Model predictive control for formation reconfiguration exploiting quasi-periodic tori in the cislunar environment, *Nonlinear Dyn.* **111**(8) (2023) 6941–6959.

[35] N. He, J. W. Du, F. N. Cheng and Z. X. Xu, Robust distributed MPC for disturbed nonlinear multi-agent systems based on a mixed differential–integral event-triggered mechanism, *J. King Saud Univ.-Comput. Inf. Sci.* **36**(1) (2024) 101915.

[36] J. Zhan, Z. P. Jiang, Y. Wang and X. Li, Distributed model predictive consensus with self-triggered mechanism in general linear multiagent systems, *IEEE Trans. Ind. Inform.* **15**(7) (2018) 3987–3997.

[37] X. X. Mi, Y. Y. Zou, S. Y. Li and H. R. Karimi, Self-triggered DMPC design for cooperative multiagent systems, *IEEE Trans. Ind. Electron.* **67**(1) (2019) 512–520.

[38] A. S. Kolarijani, S. C. Bregman, P. M. Esfahani and T. Keviczky, A decentralized event-based approach for robust model predictive control, *IEEE Trans. Autom. Control.* **65**(8) (2019) 3517–3529.

[39] Y. Y. Zou, X. Su, S. Y. Li, Y. G. Niu and D. W. Li, Event-triggered distributed predictive control for asynchronous coordination of multi-agent systems, *Automatica.* **99** (2019) 92–98.

[40] H. L. Wei, K. W. Zhang and Y. Shi, Self-triggered min–max DMPC for asynchronous multiagent systems with communication delays, *IEEE Trans. Ind. Inform.* **18**(10) (2021) 6809–6817.

[41] Z. P. Yan, J. Y. Yan, S. J. Cai, Y. Y. Yu and Y. F. Wu, Robust MPC-based trajectory tracking of autonomous underwater vehicles with model uncertainty, *Ocean Eng.* **286** (2023) 115617.

[42] L. J. Chen, B. Xiao, T. Han and H. C. Yan, Multiple time-varying formation tracking of multiple heterogeneous Euler–Lagrange systems via prescribed-time hierarchical control algorithms in task space, *Nonlinear Dyn.* **112**(5) (2024) 3643–3659.

[43] D. Limón, T. Alamo, F. Salas and E. F. Camacho, Input to state stability of min–max MPC controllers for nonlinear systems with bounded uncertainties, *Automatica* **42**(5) (2006) 797–803.

[44] L. Pan, W. Li, J. S. Zhu, Z. G. Liu, J. X. Zhao and S. N. Wang, Visual predictive control of fire monitor with time delay model of fire extinguishing jet, *Contr. Eng. Pract.* **144** (2024) 105816.

[45] Y. Dai, S. H. Yu, Y. Yan and X. H. Yu, An EKF-based fast tube MPC scheme for moving target tracking of a redundant underwater vehicle-manipulator system, *IEEE-ASME Trans. Mechatron.* **24**(6) (2019) 2803–2814.
[46] C. X. Liu, H. P. Li, J. Gao and D. M. Xu, Robust self-triggered min–max model predictive control for discrete-time nonlinear systems, *Automatica* **89** (2018) 333–339.
[47] Y. Zhang and Y. F. Su, Consensus of linear multi-agent systems under switching topology by sampled-data output feedback control, *Int. J. Robust Nonlinear Contr.* **34**(7) (2024) 8180–8204.
[48] Z. Y. Ma, H. J. Gong and X. H. Wang, Formation fault-tolerant control for multiple UAVs with external disturbances, *Aircr. Eng. Aerosp. Tec.* **96**(3) (2024) 403–416.
[49] B. Zhao, S. C. Zhang and D. R. Liu, Self-triggered approximate optimal neuro-control for nonlinear systems through adaptive dynamic programming, *IEEE Trans. Neural Netw. Learn. Syst.* (2024) 1–11.
[50] Y. Yang, H. Z. Xu and X. M. Yao, Disturbance rejection self-triggered distributed MPC with adaptive prediction horizon for asynchronous multiagent systems, *IEEE Trans. Syst. Man Cybern.-Syst.* **54**(5) (2024) 2797–2809.
[51] Q. Q. Yang, J. Li, X. Feng, S. Wu and F. Gao, Event-triggered consensus for second-order multi-agent systems via asynchronous periodic sampling control approach, *Int. J. Control Autom. Syst.* **18** (2020) 1399–1411.

Zheping Yan received his B.S. degree in nuclear engineering form Harbin Engineering University, Harbin, China, in 1994; received his M.S. degree in ship and ocean engineering special auxiliary devices and systems form Harbin Engineering University, Harbin, China, in 1997, and Ph.D. degree in control science and engineering form Harbin Engineering University, Harbin, China, in 2001. He is now the director of the Engineering Research Center of the Ministry of Education for Ship Control Engineering of Harbin Engineering University, and has published more than 130 SCI and EI search papers and one monograph. He is currently engaged in the research of overall optimization design, underwater intelligence, integrated testing, and environmental applications of underwater unmanned systems and submarines. He has presided over and completed 13 projects of NSFC, New Century Talent Support, Provincial Outstanding Youth Fund, etc. He is also working on 2 projects: participating in NSFC national major scientific research instrument development project and presiding over a national model development project.

Jinyu Yan received his B.S. degree in automation from Harbin Engineering University, Harbin, China, in 2020, and is currently pursuing Ph.D. degree in control science and engineering at Harbin Engineering University. His main research is on trajectory tracking and formation control of unmanned underwater vehicles (UUVs), as well as path planning.